



Article

# Polyfunctional Sterically Hindered Catechols with Additional Phenolic Group and Their Triphenylantimony(V) Catecholates: Synthesis, Structure, and Redox Properties

Ivan V. Smolyaninov <sup>1,2</sup> , Andrey I. Poddel'sky <sup>3,\*</sup> , Susanna A. Smolyaninova <sup>2</sup>, Maxim V. Arsenyev <sup>3</sup>, Georgy K. Fukin <sup>3</sup> and Nadezhda T. Berberova <sup>2</sup>

<sup>1</sup> Toxicology Research Group, Federal State Budgetary Institution of Science “Federal Research Centre The Southern Scientific Centre of the Russian Academy of The Sciences”, Tatischeva str. 16, 414056 Astrakhan, Russia; ivsmolyaninov@gmail.com

<sup>2</sup> Department of Chemistry, Astrakhan State Technical University, 16 Tatischeva str., Astrakhan 414056, Russia; zeynalovasa@mail.ru (S.A.S.); nberberova@gmail.com (N.T.B.)

<sup>3</sup> G.A. Razuvaev Institute of Organometallic Chemistry, Russian Academy of Sciences, 49 Tropinina str., 603137 Nizhny Novgorod, Russia; mars@iomc.ras.ru (M.V.A.); gera@iomc.ras.ru (G.K.F.)

\* Correspondence: aip@iomc.ras.ru; Tel./Fax: +7-831-462-7497

Academic Editor: Vito Lippolis

Received: 27 March 2020; Accepted: 10 April 2020; Published: 12 April 2020



**Abstract:** New polyfunctional sterically hindered 3,5-di-*tert*-butylcatechols with an additional phenolic group in the sixth position connected by a bridging sulfur atom—(6-(CH<sub>2</sub>-S-*t*Bu<sub>2</sub>Phenol)-3,5-DBCat)H<sub>2</sub> (**L**<sub>1</sub>), (6-(S-*t*Bu<sub>2</sub>Phenol)-3,5-DBCat)H<sub>2</sub> (**L**<sub>2</sub>), and (6-(S-Phenol)-3,5-DBCat)H<sub>2</sub> (**L**<sub>3</sub>) (3,5-DBCat is dianion 3,5-di-*tert*-butylcatecolate)—were synthesized and characterized in detail. The exchange reaction between catechols **L**<sub>1</sub> and **L**<sub>3</sub> with triphenylantimony(V) dibromide in the presence of triethylamine leads to the corresponding triphenylantimony(V) catecholates (6-(CH<sub>2</sub>-S-*t*Bu<sub>2</sub>Phenol)-3,5-DBCat)SbPh<sub>3</sub> (**1**) and (6-(S-Phenol)-3,5-DBCat)SbPh<sub>3</sub> (**2**). The electrochemical properties of catechols **L**<sub>1</sub>–**L**<sub>3</sub> and catecholates **1** and **2** were investigated using cyclic voltammetry. The electrochemical oxidation of **L**<sub>1</sub>–**L**<sub>3</sub> at the first stage proceeds with the formation of the corresponding *o*-benzoquinones. The second process is the oxidation of the phenolic moiety. Complexes **1** and **2** significantly expand their redox capabilities, owing to the fact that they can act as the electron donors due to the catecholate metallocycle capable of sequential oxidations, and as donors of the hydrogen atoms, thus forming a stable phenoxyl radical. The molecular structures of the free ligand **L**<sub>1</sub> and complex **1** in the crystal state were determined by single-crystal X-ray analysis.

**Keywords:** redox-active ligand; catechol; thioether; antimony; X-ray; cyclic voltammetry; electronic paramagnetic resonance

## 1. Introduction

A large amount of data has been accumulated to the present time on the complexes of transition and non-transition elements with redox active ligands: *o*-benzoquinones, *o*-iminobenzoquinones and alpha-diimines [1–11]. A feature of these compounds is the participation of not only metal but also redox-active ligands in the processes of electron transfer and, as a result, they are capable of reversible accepting and donating electrons during the different chemical transformations, while remaining bound to the metal. This feature can significantly expand or change the reactivity of metal complexes. Studies of non-transition metal complexes containing redox-active ligands of the *o*-quinonato type have allowed to reveal an expansion of the valence potentials of non-transition metals

due to redox-active ligands [12,13], to observe of the phenomenon of redox isomerism in the main group metals' chemistry [14], and also to observe and investigate the ability of antimony(V) complexes to reversible fixation of molecular oxygen [15–19], to observe the fixation of nitrogen(II) oxide (by zinc(II) and lead(II) catecholates) [20].

There are several approaches that allow to change the properties of ligands and their metal complexes: (1) a modification of the ligands' structure by the variation of heteroatoms (O, N, S) or the presence of bulky organic substituents; (2) the introduction of different electron donor/acceptor groups or additional redox-active as well as chelating fragments at various positions of the quinoid ring; and (3) a combination of a redox-active ligand and an additional coordination center. Organic and organometallic compounds containing several redox centers are of particular interest in view of a number of their specific features: the possibility of indirect activation through certain functional groups, intramolecular electron transfer, proton-conjugated electron transfer, etc. From the example of ferrocene derivatives (ferrocifenes) as well as quinoid compounds, it was shown that various types of biological activities (cytotoxicity, antibacterial, antiparasitic, antioxidant) depend directly on the presence of a redox-active group and its transformations [21–24]. Redox-asymmetric systems can be built not only on the basis of a ferrocenyl fragment but also on a combination of phenolic, amide, and amino groups, which are also of interest because of the possibility of proton-conjugated charge transfer reactions [25–27].

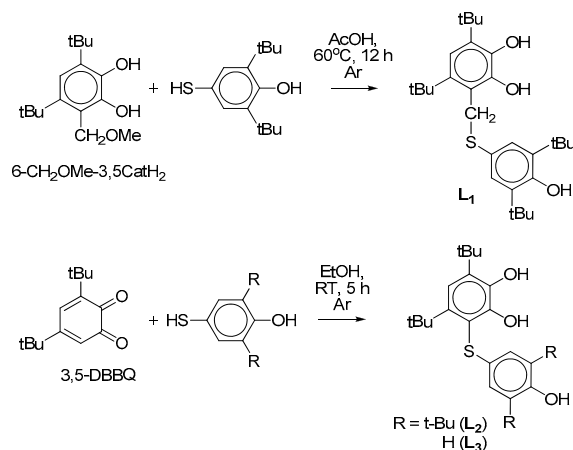
For a long time, dioxolenes have attracted the attention of researchers because of the possibility of their existence in several redox states. Recently, the focus of research in this area has been aimed at their functionalization by introducing additional redox-active groups [28–31] or coordination sites [32–35]. In the series of functionalized derivatives of catechol/*o*-quinones, sulfur-containing compounds occupy a special place since sulfide bridge fragments also exhibit redox activity. The introduction of the tetrathiafulvalene linker allows to obtain bis-quinones and their metal complexes which exhibit unusual physicochemical properties [36–39]. The sterically hindered dithiete-annulated *o*-benzoquinone is a bifunctional ligand, which combines two chalcogen redox-active coordination centers in its structure—dioxolene and dithiolene—allowing it to form complexes in which various coordination sites are involved [40]. S-functionalization of 3,5-di-*tert*-butyl-*o*-benzoquinone with cystamine and cysteine has made it possible to obtain Cu(II), Zn(II), and Ni(II) complexes [41,42]. A similar reaction with dithiols makes it possible to synthesize catechols with a free thio group or bis-catechol thioethers [43,44], which have chelating properties and the ability to be absorbed on the surface [45–47]. Variation of the organic groups in thiols allows one to obtain a wide range of thiolated catechols, which exhibit antioxidant, antiradical, and cryoprotective activity [48–50]. Transition metal compounds based on sulfur-containing catecholate/*o*-semiquinolate ligands demonstrate antifungal and antibacterial activity [51,52]. Thus, the synthesis and study of the properties of thiolated dioxolene ligands and metal complexes based on them is relevant in view of the diversity of the properties manifested. Antimony(III/V) derivatives are used as antiparasitic agents in the treatment of leishmaniasis [53], and have potential as antitumor, cytotoxic, and antibacterial substances [54,55]. Along with biological activity, antimony complexes are promising compounds for the design of functional materials. The presence of a catecholate cycle at the antimony atom allows the creation of new colorimetric and fluorescent sensors for the fluoride anion [56–59]. The polymer compositions containing catecholate derivatives of triphenylantimony(V) are promising for the creation of polymeric materials capable of fixing oxygen [60–62].

In the present paper, we report on new thioethers combining several redox-active centers: A chelating catechol fragment, a phenolic group, and a thioether linker. The coordinating activity of the catechol fragment was studied in a reaction with triphenylantimony(V) dibromide, and as a result, triphenylantimony(V) catecholates, which contain redox-active centers of a different nature, were synthesized. The molecular structure and electrochemical transformations of the resulting compounds are discussed.

## 2. Results and Discussion

### 2.1. Synthesis and Characterization

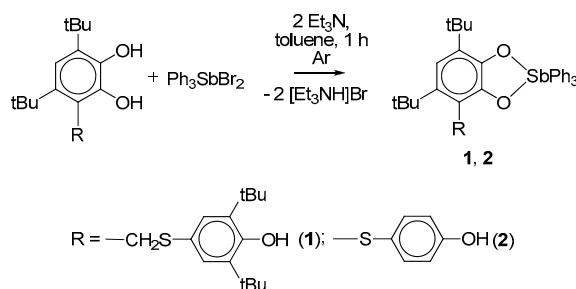
The sterically hindered catechol (6-(CH<sub>2</sub>-S-tBu<sub>2</sub>Phenol)-3,5-DBCat)H<sub>2</sub> (**L**<sub>1</sub>) was synthesized from 6-methoxymethyl-3,5-di-*tert*-butylcatechol (6-CH<sub>2</sub>OMe-3,5-Cat)H<sub>2</sub> and 2,6-di-*tert*-butyl-4-mercaptophenol in a solution of acetic acid at 60°C (Scheme 1(1)). The 3,5-di-*tert*-butylcatechols (6-(S-tBu<sub>2</sub>Phenol)-3,5-DBCat)H<sub>2</sub> (**L**<sub>2</sub>) and (6-(S-Phenol)-3,5-DBCat)H<sub>2</sub> (**L**<sub>3</sub>) were prepared by the reaction of 3,5-di-*tert*-butyl-*o*-benzoquinone with 2,6-di-*tert*-butyl-4-mercaptophenol or 4-mercaptophenol [48], respectively, in ethanol solution (Scheme 1(2)).



**Scheme 1.** Synthesis of catechols **L**<sub>1</sub>–**L**<sub>3</sub>.

Catechols **L**<sub>1</sub>, **L**<sub>2</sub> were isolated as pale-yellow microcrystalline powders that were well-soluble in toluene or chloroform. The composition of these catechols was determined by means of IR-, <sup>1</sup>H-, and <sup>13</sup>C{<sup>1</sup>H} NMR spectroscopy and elemental analysis. A prolonged recrystallization of **L**<sub>1</sub> from n-hexane allowed X-ray-quality white crystals of **L**<sub>1</sub> to be grown.

A substitution reaction between catechols **L**<sub>1</sub> or **L**<sub>3</sub> and triphenylantimony(V) dibromide in the presence of two equivalents of triethylamine in toluene solution leads to the corresponding triphenylantimony(V) catecholates (Scheme 2).



**Scheme 2.** Synthesis of complexes **1** and **2**.

Complexes **1** and **2** were isolated as yellow solids. These compounds are readily soluble in common organic solvents, such as aliphatic or aromatic hydrocarbons, chloroform, ethers, and methanol. Complexes **1** and **2** were characterized by IR-, <sup>1</sup>H-, and <sup>13</sup>C{<sup>1</sup>H} NMR spectroscopy and elemental analysis. The X-ray suitable crystals of **1** were grown by the prolonged (during 5 days) crystallization of complex in toluene solution at −18°C.

## 2.2. Molecular Structures

The molecular structure of catechol **L**<sub>1</sub> in crystal is shown on Figure 1. The general geometrical parameters of catechol fragment are typical for this class of compounds. The carbon–carbon bonds in a ring C(1–6) have an average distance of  $1.401 \pm 0.014$  Å, which is typical of aromatic systems. The carbon–oxygen distances are ordinary [63] and close to each other: the bonds O(1)–C(1), O(2)–C(2), and O(3)–C(11) are 1.3816(14), 1.3804(14), and 1.3806(14) Å, respectively. The molecule is not planar, the angle between catechol and phenolic aromatic rings planes is equal to  $54.7(1)^\circ$ , the torsion angle is  $47.9(1)^\circ$ , and the torsion angle C(1)C(6)C(7)S(1) is  $56.7(1)^\circ$ . Such distortion of geometry is supported by an intramolecular hydrogen bonding in the molecule: the distance O(2)–H(2) ... O(1) is 2.07(1) Å, angle O(2)–H(2)–O(1) is  $126.6(1)^\circ$ , and the distance O(1)–H(1) ... S(1) is 2.28(1) Å, angle O(1)–H(1)–S(1) is  $153.0(1)^\circ$ . In the crystal, molecules form pairs due to the intermolecular hydrogen bonding between phenolic hydroxyl groups (Figure S9). The intermolecular distances O(3)–H(3) ... O(3') are 1.71(1) Å, and the corresponding angles O(3)–H(3)–O(3') are  $113.5(1)^\circ$ . The distance between the planes of catecholate rings in neighboring pairs is 3.49(1) Å, which is close to the sum of the Van der Waals radii of carbon atoms [64].

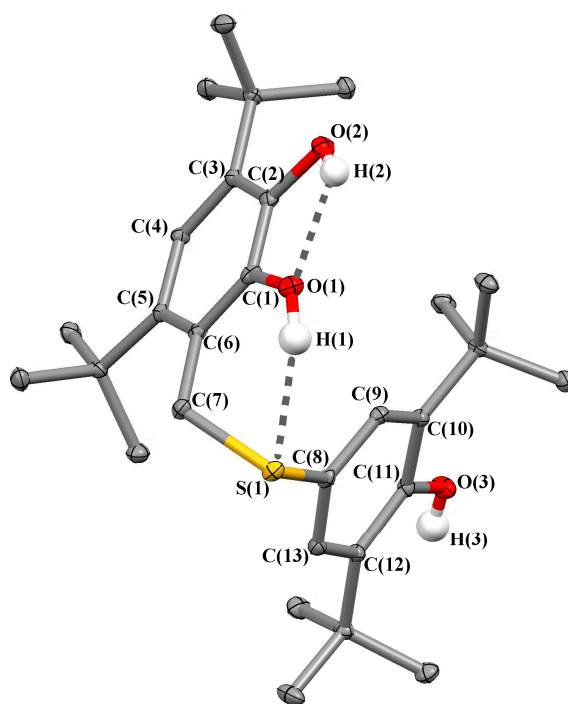


**Figure 1.** The X-ray structure of catechol **L**<sub>1</sub> (6-(CH<sub>2</sub>-S-tBu<sub>2</sub>Phenol)-3,5-DBCat)<sub>2</sub>H<sub>2</sub> in crystal. The hydrogen atoms except hydroxyl hydrogens are omitted for clarity. The ellipsoids of 50% probability. The selected bond distances (Å): O(1)–C(1) 1.3816(14), O(2)–C(2) 1.3804(14), O(3)–C(11) 1.3806(14), S(1)–C(7) 1.8527(12), S(1)–C(8) 1.7765(11), C(1)–C(2) 1.3967(16), C(1)–C(6) 1.3987(16), C(2)–C(3) 1.3910(16), C(3)–C(4) 1.4029(15), C(4)–C(5) 1.4016(15), C(5)–C(6) 1.4150(15), C(6)–C(7) 1.5101(15), C(8)–C(9) 1.3907(16), C(8)–C(13) 1.3893(16), C(9)–C(10) 1.3947(16), C(10)–C(11) 1.4118(15), C(11)–C(12) 1.4139(15), C(12)–C(13) 1.3949(16).

The molecular structure of triphenylantimony(V) catecholate **1** in crystal is shown in Figure 2. The central antimony atom Sb(1) has a distorted square pyramidal geometry with an O,O'-chelating ligand and two phenyl groups in the basal plane. The bond angles in the base of pyramid O(1)–Sb(1)–C(30) and O(2)–Sb(1)–C(36) are  $156.73(6)^\circ$  and  $142.01(7)^\circ$ . The bond Sb(1)–C(42) with the apical phenyl group is approximately 0.028(2)–0.033(2) Å shorter than the equatorial bonds Sb(1)–C(30) and Sb(1)–C(36). The planes of the aromatic rings C(16–21) and C(1–6) of the phenolic group and the catecholate ligand, respectively, lie at an angle of  $57.6(1)^\circ$ . The arylthio-fragment in **1** is stronger turned away from the

catechol ring than in catechol  $L_1$ , the torsion angle C(2)C(3)C(7)S(1) in **1** is  $77.9(1)^\circ$  (vs.  $56.7(1)^\circ$  in  $L_1$ ), and the torsion angle C(3)C(7)S(1)C(16) is  $138.1(1)^\circ$  (vs.  $47.9(1)^\circ$  in  $L_1$ ).

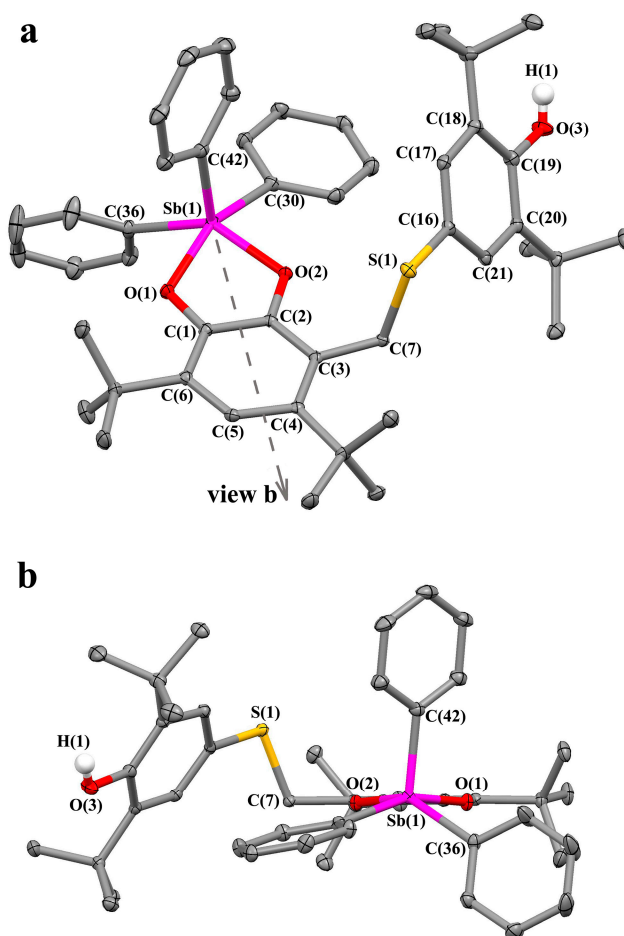


**Figure 2.** The X-ray structure of **1**: (a) the general view on molecule of **1**; (b) the view on molecule **1** along the dotted line (view b) depicted on Figure 2a. The hydrogen atoms except hydroxyl hydrogen H(1) are omitted for clarity. The ellipsoids of 50% probability. The selected bond distances (Å): Sb(1)–O(1) 2.0402(13), Sb(1)–O(2) 2.0256(13), Sb(1)–C(30) 2.1328(19), Sb(1)–C(36) 2.1383(19), Sb(1)–C(42) 2.1054(19), O(1)–C(1) 1.358(2), O(2)–C(2) 1.366(2), O(3)–C(19) 1.376(2), O(3)–H(1) 0.73(3), S(1)–C(7) 1.8365(18), S(1)–C(16) 1.7772(19), C(1)–C(2) 1.398(3), C(1)–C(6) 1.393(3), C(2)–C(3) 1.392(3), C(3)–C(4) 1.415(3), C(4)–C(5) 1.400(3), C(5)–C(6) 1.401(3), C(16)–C(17) 1.385(3), C(16)–C(21) 1.389(3), C(17)–C(18) 1.394(3), C(18)–C(19) 1.413(3), C(19)–C(20) 1.408(3), C(20)–C(21) 1.390(3).

The oxygen-to-carbon bonds O(1)–C(1) and O(2)–C(2) (1.358(2) and 1.366(2) Å, respectively) are ordinary and typical for catecholato complexes of different metals [65], and bond O(3)–C(19) (1.376(2) Å) is the longest O–C bond in **1**, which is typical for sterically hindered phenols [66–68]. The six-membered carbon ring C(1)–C(6) is aromatic, with average C–C bond distances of  $1.400 \pm 0.015$  Å, which is very close to the same value for catechol  $L_1$ . In general, the geometrical characteristics of the redox-active catecholato ligand in **1** are typical for various antimony(V) catecholates [69–79].

In the crystal, molecules **1** form layers, where one can find intermolecular hydrogen bonding between the phenol group of one complex molecule and the sulfur atom of a neighboring complex molecule (Figure S10) with a distance O(3)–H(1) ... S(1) of 2.86(1) Å and corresponding angle O(3)–H(1)–S(1) of  $115.5(1)^\circ$ .

### 2.3. Electrochemistry

The electrochemical properties of catechol thioethers **L**<sub>1</sub>–**L**<sub>3</sub> and triphenylantimony(V) catecholate complexes **1**, **2** were investigated by cyclic voltammetry (CV) in CH<sub>2</sub>Cl<sub>2</sub> and MeCN solutions containing 0.15 M NBu<sub>4</sub>ClO<sub>4</sub> (TBAP) as the supporting electrolyte at a glassy carbon working electrode. The redox potentials given in Table 1; Table 2 are referenced to Ag/AgCl/KCl(sat.) electrode.

**Table 1.** The CV data for thioethers **L**<sub>1</sub>–**L**<sub>3</sub> and triphenylantimony(V) catecholates **1** and **2** in CH<sub>2</sub>Cl<sub>2</sub> (GC anode, C = 3·10<sup>−3</sup> M, Ar, 0.15 M Bu<sub>4</sub>NClO<sub>4</sub>, vs. Ag/AgCl/KCl(sat.)).

Compound	E <sup>ox1</sup> , V <sup>1</sup>	I <sub>c</sub> /I <sub>a</sub>	E <sup>ox2</sup> , V <sup>1</sup>	I <sub>c</sub> /I <sub>a</sub>	E <sup>ox3</sup> , V
<b>L</b> <sub>1</sub>	1.28	-	1.49	-	-
<b>L</b> <sub>2</sub>	1.37 (1.32)	0.4	1.58 (1.55)	0.6	1.77
<b>L</b> <sub>3</sub>	1.28	-	1.48	-	-
<b>1</b>	0.96 (0.89)	0.8	1.39 (1.27)	0.5	-
<b>2</b>	1.04 (0.96)	0.7	1.24	-	1.48

<sup>1</sup> The half-wave potentials E<sub>1/2</sub> for quasi-reversible oxidation processes are given in parentheses.

**Table 2.** The CV data for thioethers **L**<sub>1</sub>–**L**<sub>3</sub> and triphenylantimony(V) catecholates **1** and **2** in CH<sub>3</sub>CN (GC anode, C = 3·10<sup>−3</sup> M, Ar, 0.15 M Bu<sub>4</sub>NClO<sub>4</sub>, vs. Ag/AgCl/KCl(sat.)).

Compound	E <sup>ox1</sup> , V <sup>1</sup>	I <sub>c</sub> /I <sub>a</sub>	E <sup>ox2</sup> , V <sup>1</sup>	I <sub>c</sub> /I <sub>a</sub>	E <sup>ox3</sup> , V
<b>L</b> <sub>1</sub>	1.09	-	1.34	-	1.69
<b>L</b> <sub>2</sub> *	1.27	-	1.48	0.3	-
<b>L</b> <sub>3</sub> **	1.13	-	1.26	-	1.61
<b>1</b>	0.89 (0.84)	0.4	1.23 (1.12)	0.5	1.68
<b>2</b>	0.94 (0.89)	0.8	1.36	-	-

<sup>1</sup> The half-wave potentials E<sub>1/2</sub> for quasi-reversible oxidation processes are given in parentheses. \* Data have been received in a mixture “CH<sub>3</sub>CN/ CH<sub>2</sub>Cl<sub>2</sub>” (2:1). \*\* Data from ref. [48].

Compounds **L**<sub>1</sub>–**L**<sub>3</sub> are characterized by the presence of multiple electroactive fragments: catechol, phenolic group, and thioether linker, which affects their electrochemical behavior. The electrooxidation of the target catechol thioethers occurs in three or two successive stages depending on the applied solvent. Figure 3 shows the cyclic voltammograms (CVs) of **L**<sub>1</sub> in acetonitrile solution. The CV of **L**<sub>1</sub> in dichloromethane is shown in Figure S11 of ESI. The first two-electron electrochemical stage is ascribed to the irreversible oxidation of the catechol fragment in the case of compounds **L**<sub>1</sub> and **L**<sub>3</sub>. A similar behavior is typical for substituted catechols in aprotic solvents: 3,5-di-*tert*-butylcatechol has an irreversible oxidation peak at 1.11 (CH<sub>3</sub>CN) or 1.23 V (CH<sub>2</sub>Cl<sub>2</sub>). In the first stage, the mechanism of electrooxidation involves electron transfer followed by fast deprotonation, leading to *o*-quinone formation (Scheme 3).

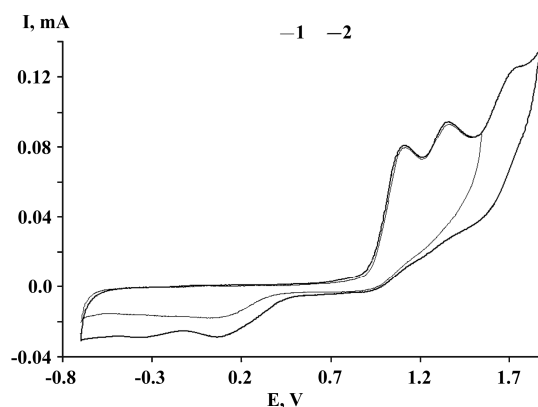
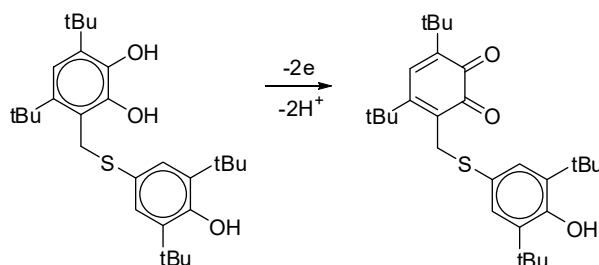


**Figure 3.** Cyclic voltammograms of compound **L**<sub>1</sub> (in the potential switch from  $-0.70$  to  $1.5$  V—curve 1; in the potential switch from  $-0.70$  to  $1.85$  V—curve 2) (MeCN,  $C = 3$  mM,  $0.15$  M TBAP, scan rate  $200$   $\text{mV}\cdot\text{s}^{-1}$ ).



**Scheme 3.** The first stage of electrochemical oxidation of **L**<sub>1</sub>.

Earlier spectroelectrochemical investigations of catechol **L**<sub>3</sub> have shown that electrolysis at the controlled potential leads to the formation of the corresponding *o*-benzoquinone [48]. The formation of the *o*-quinone structure is accompanied by the appearance of a wide absorption band at  $400$ – $500$  nm. A wide absorption band in the visible spectral range is a characteristic feature of compounds containing a quinoid fragment [80]. The spectroelectrochemistry of **L**<sub>1</sub> under the controlled potential electrolysis also confirms the formation of the corresponding *o*-benzoquinone.

As a result of electrooxidation, new absorption with a maximum at  $410$  nm was observed in the visible region of the spectrum and the intensity of this band increased with time (Figure 4). Additionally, the second characteristic band of lower intensity in the form of a shoulder to the main band appears in the region of  $590$  nm, which corresponds to the  $n$ - $\pi^*$  transition in quinones.

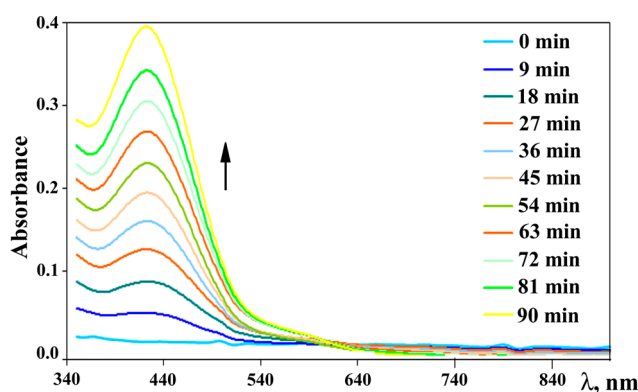


**Figure 4.** The changes in the absorption spectrum of thioether **L**<sub>1</sub> during the electrolysis time (90 min) at a controlled potential  $1.2$  V (MeCN, Ar,  $C = 0.5$  mM,  $0.15$  M TBAP).



The absorption band in the visible spectral range corresponds to a  $\pi$ - $\pi^*$  transition, which is a characteristic for compounds containing a quinonoid fragment like 3,5-di-*tert*-butyl-*o*-benzoquinone [81]. The CV of **L**<sub>1</sub> after electrolysis in the cathodic region contains a quasi-reversible peak at  $E_{1/2} = -0.58$  V (Figure S12 of ESI). This peak is assigned to the reduction of electrogenerated *o*-benzoquinone to *o*-benzosemiquinone.

The second oxidation peak on CVs of catechols **L**<sub>1</sub>, **L**<sub>3</sub> may be assigned to the oxidation of the phenolic group. In acetonitrile, for compounds **L**<sub>1</sub> and **L**<sub>3</sub>, the shift of the second oxidation potential to the cathode region occurs as compared to the oxidation of the well-known phenolic antioxidant (ionol)—2,6-di-*tert*-butyl-4-methylphenol 1.47 V (CH<sub>3</sub>CN). In dichloromethane, the oxidation potentials of **L**<sub>1</sub> and **L**<sub>3</sub> are close to the value for this phenolic compound (1.48 V). The presence of the thioether group causes the appearance of the third redox wave at high anodic potentials. For **L**<sub>1</sub> and **L**<sub>3</sub> in acetonitrile, the values  $E^{\text{ox}3}$  are in good agreement with the data on the oxidation of catechol thioethers: the electrooxidation of the thioether group occurs in the potential range from 1.59 to 1.67 V. On the CVs of **L**<sub>1</sub>, **L**<sub>3</sub> in dichloromethane, two oxidation waves only are observed and they are shifted to the anodic region by 0.15 and 0.19 V in comparison with the data in MeCN. Obviously, the third anode process occurs at the higher anodic potential restricted by the electrochemical oxidation of the solvent.

The CV of **L**<sub>2</sub> in dichloromethane solution has three oxidation peaks like the CVs of **L**<sub>1</sub> and **L**<sub>3</sub> in acetonitrile (Figure 5).

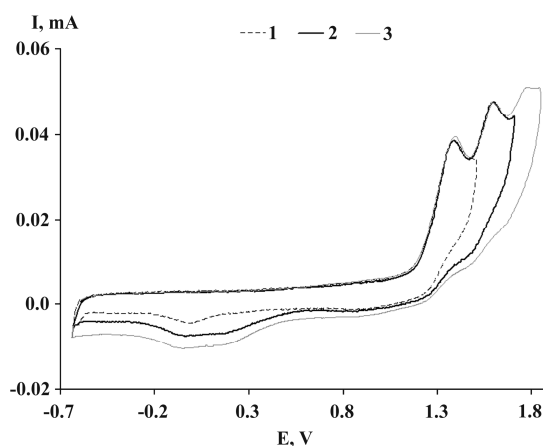
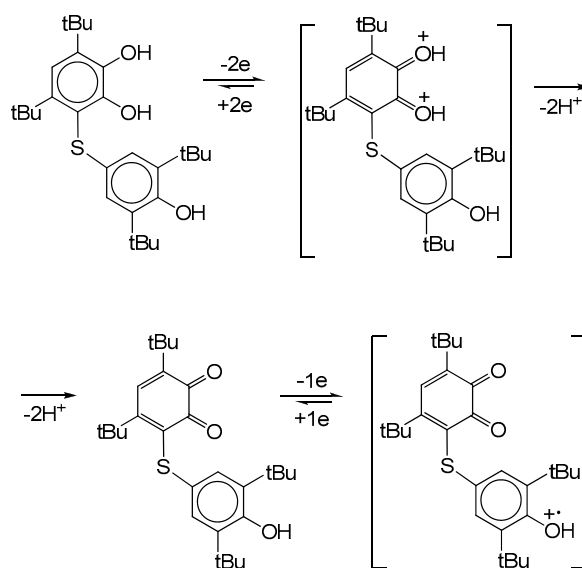


**Figure 5.** The CV curves of **L**<sub>2</sub> (in the potential switch from  $-0.60$  to  $1.50$  V—curve 1; in the potential switch from  $-0.60$  to  $1.70$  V—curve 2; in the potential switch from  $-0.60$  to  $1.85$  V—curve 3) (CH<sub>2</sub>Cl<sub>2</sub>,  $C = 1.5$  mM,  $0.15$  M TBAP, scan rate  $200$  mV·s<sup>-1</sup>).

In contrast to the above described catechol-thioesters **L**<sub>1</sub> and **L**<sub>3</sub>, the first and second oxidation stages for compound **L**<sub>2</sub> are quasi-reversible. The obtained values of the current ratio ( $I_c/I_a$ ) indicate a low stability of the electrically generated intermediates. The introduction of *tert*-butyl groups helps to stabilize the dication formed in the first stage (like in the case of **L**<sub>1</sub>); however, nevertheless, a rapid deprotonation reaction occurs in the solution, and, as a result, a small reduction peak is observed in the reverse scan of CV. At the second stage, one-electron oxidation of a sterically hindered phenolic fragment leads to the formation of a cation-radical intermediate, which is more stable over the time of the CV experiment (Scheme 4).



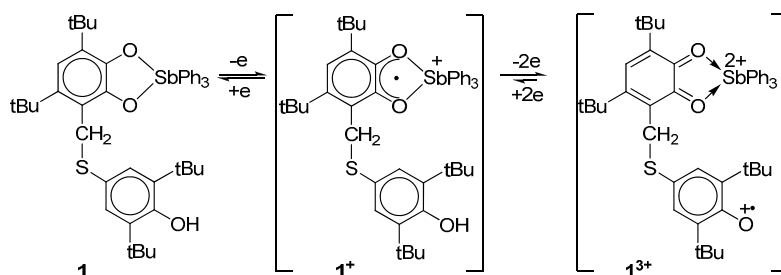


**Scheme 4.** The electrochemical oxidation of  $L_2$ .

The third anode peak at the potential of 1.77 V suggests the participation of the thioether fragment in further redox transformations.

It should be noted that the presence of an electron-withdrawing sulfur atom in the catecholite ring or the presence of a methylene bridge between the aromatic ring and the heteroatom does not practically affect the oxidation potentials of compounds  $L_1$  and  $L_3$  in dichloromethane (Table 1). At the same time, the first oxidation potential (0.05 V) for  $L_3$  is shifted to the anode region as compared with 3,5-di-*tert*-butylcatechol in accordance with the electro-acceptor effect of the sulfur atom. In acetonitrile, such changes are less pronounced. In dichloromethane, for compounds  $L_2$  and  $L_3$ , which differ by the absence or presence of *tert*-butyl groups in the phenolic fragment, a shift of the oxidation potentials (0.11 and 0.10 V) for  $L_2$  to the anode region is observed. This behavior can be rationalized by the formation of stronger intramolecular hydrogen bonds between the catechol hydroxyl and the sulfur atom than in the case of compound  $L_1$ . Using S-functionalized phenols as an example, such an interaction led to an increase in the bond-breaking energy, BDE (O-H) [82]. The 4-hydroxyphenylthio group introduced into the catecholite cycle exhibits an electron-withdrawing effect, which is expressed for  $L_2$  in a significant shift (0.14 V) of the first oxidation potential to the anode region as compared with 3,5-di-*tert*-butylcatechol.

As in the case of free ligands, the solvent has a significant effect on the electrochemical behavior of complexes **1** and **2**. In dichloromethane, for both complexes, the first stage of oxidation has a quasi-reversible one-electron character and leads to the formation of relatively stable (in the CV time scale) monocationic complexes of the type  $[(SQ)SbPh_3]^+$  (Scheme 5) [83,84]. The value of the  $E^{ox1}_{1/2}$  potential for **1** is similar to the data obtained for triphenylantimony(V) 3,6-di-*tert*-butylcatecholite [85]. For the complex **2**, this value shifts by 0.06 V to the anode region, which is associated with the electron-withdrawing effect of the sulfur atom, which is not separated from the catecholite ring by the methylene group as in case of **1**. Such changes are in good agreement with previously obtained results for triarylantimony(V) 6-chloro(bromo)-3,5-di-*tert*-butylcatecholites [86,87]. The introduction of a methylene group between the catecholite fragment and the 3,5-di-*tert*-butyl-4-hydroxyphenylthio group has no practically effect on the value of the  $E^{ox1}_{1/2}$  potential, as in the case of 6-alkoxymethyl-substituted 3,5-di-*tert*-butylcatecholites of triphenylantimony(V) [88].



**Scheme 5.** The electrochemical oxidation of complex 1.

For complex 1, the second anode peak has a quasi-reversible character (Figure 6). A double increase in the current of the second oxidation peak as compared to the first one indicates an increase in the number of electrons involved in this electrode process to two.

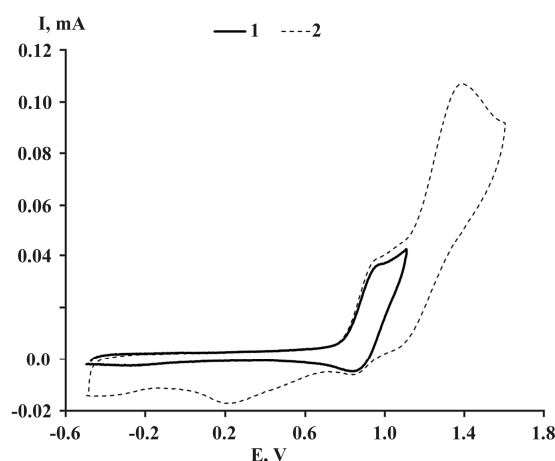
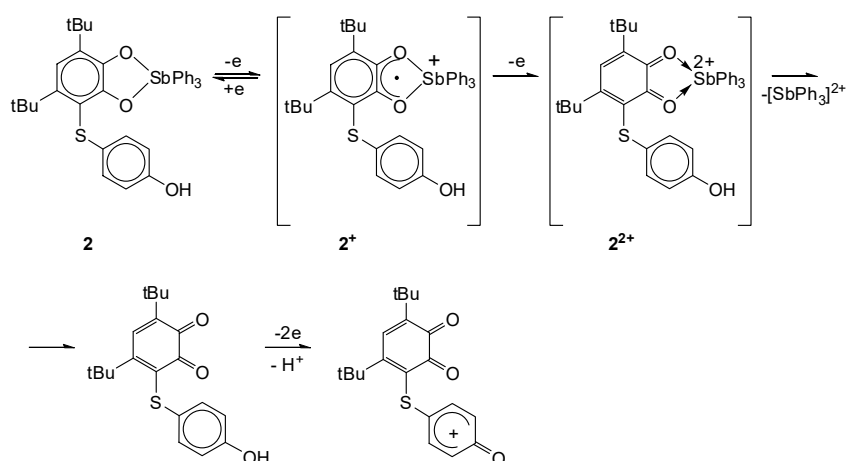


**Figure 6.** Cyclic voltammograms of compound 1 (in the potential switch from  $-0.5$  to  $1.1$  V—curve 1; in the potential switch from  $-0.5$  to  $1.6$  V—curve 2) ( $\text{CH}_2\text{Cl}_2$ ,  $C = 3$  mM,  $0.15$  M TBAP, scan rate  $200$   $\text{mV}\cdot\text{s}^{-1}$ ).

The value of the peak potential  $E^{\text{ox}2}_{\text{p}} = 1.39$  V on the CV of 1 is fixed in the potential range of  $1.37$ – $1.60$  V, which is characteristic of the second redox process “*o*-semiquinone/*o*-benzoquinone” in such triarylsantimony(V) catecholates [89–91]. This electrochemical picture in the case of 1 indicates the convergence of the boundary redox orbitals of *o*-semiquinone and phenolic fragments in 1<sup>•+</sup>, which leads to their simultaneous electrooxidation. A decrease in the ratio of currents to 0.5 for the second oxidation process is caused by the subsequent chemical stages in the solution—deprotonation of the phenoxyl radical cation and decooordination of *o*-benzoquinone moiety from the tricationic intermediate.

In complex 2, these redox centers behave separately: The second oxidation stage at  $1.24$  V is irreversible and assigned to the further oxidation of coordinated *o*-benzosemiquinone in the intermediate  $[(\text{SQ})\text{SbPh}_3]^+$  (2<sup>•+</sup>) to *o*-benzoquinone, with the subsequent decooordination of *o*-benzoquinone from 2<sup>•+</sup> leading to the complex decomposition (Scheme 6). The third redox process is a two-electronic peak, which is an oxidation of the phenolic group in free *o*-benzoquinone at  $1.48$  V (Figure 7).



**Scheme 6.** The electrochemical oxidation of complex **2**.

The potential value of this third redox-stage is identical with that one for the oxidation of the phenolic group in free **L**<sub>3</sub> and 2,6-di-*tert*-butyl-4-methylphenol (1.48 V vs. Ag/AgCl) [92].

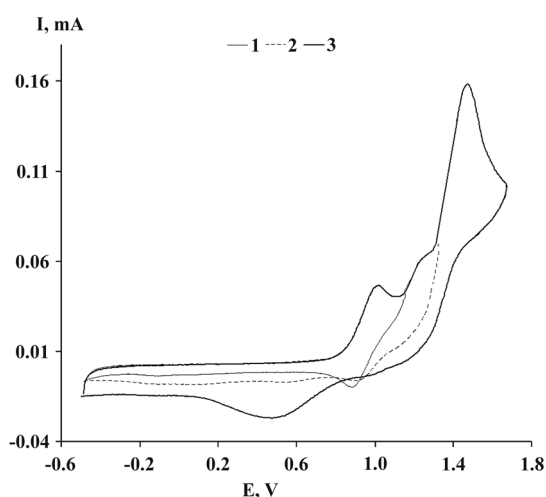
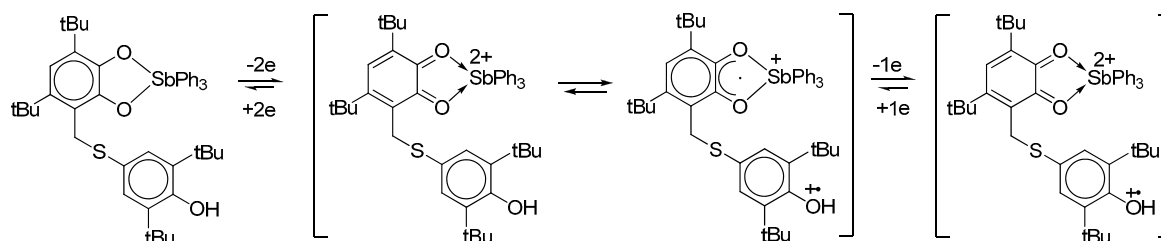


**Figure 7.** Cyclic voltammograms of compound **2** (in the potential switch from  $-0.50$  to  $1.15$  V—curve 1; in the potential switch from  $-0.50$  to  $1.30$  V—curve 2; in the potential switch from  $-0.50$  to  $1.70$  V—curve 3) ( $\text{CH}_2\text{Cl}_2$ ,  $C = 3$  mM,  $0.15$  M TBAP, scan rate  $200$   $\text{mV}\cdot\text{s}^{-1}$ ).

In a coordinating solvent acetonitrile (Table 2), the oxidation potentials for complexes **1** and **2**, as it was expected, shift slightly to the cathode region. In the whole, the electrochemical behavior of the complexes changes. The CV of **1** in acetonitrile has three oxidation waves (Figure S13).

In acetonitrile, the current of the first quasi-reversible oxidation peak for **1** increases twice to a two-electron level, and the ratio of currents  $I_c/I_a$  decreases in comparison with the data obtained for **1** in dichloromethane. These changes indicate the generation of an unstable dicationic intermediate  $[(\text{Q})\text{SbPh}_3]^{2+}$  in the near-electrode region. Earlier, we observed a similar electrochemical activity for the triphenylantimony(V) catecholates containing electron-withdrawing groups in the catecholate cycle, but in most cases, the dicationic derivatives formed in the electrooxidation were unstable [90,91]. The second wide quasi-reversible oxidation peak at  $1.24$  V is single electron in nature. The low value of the current ratio, as in the first case, indicates the instability of the resulting intermediate and the course of the subsequent chemical stage. The proximity of the redox orbitals of the catecholate ligand and the sterically hindered phenol fragment does not allow us to unambiguously describe the oxidative transformations at the first and second stages of oxidation. Based on the value of the

first oxidation potential, we may assume that the dianionic catecholate fragment is oxidized initially to *o*-benzoquinone, accompanied by an electron transfer from the phenolic group to the dication (Scheme 7). The second anode process may equally be attributed to the oxidation of a coordinated *o*-semiquinone radical anion to *o*-benzoquinone or to the oxidation of a di-*tert*-butylphenol moiety to a radical cation.



**Scheme 7.** The electrochemical oxidation of complex **1** in acetonitrile.

The electrooxidation of **2** in acetonitrile (Figure 8) has a quasi-reversible one-electron character at the first stage (as in dichloromethane), which indicates the generation of a monocation complex containing a coordinated *o*-semiquinone ligand.

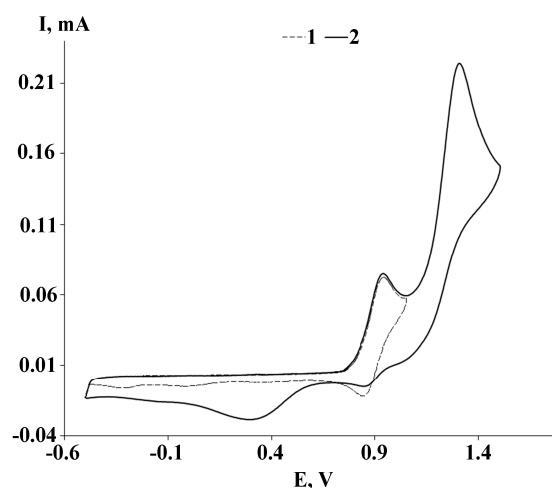


**Figure 8.** Cyclic voltammograms of compound **2** (in the potential switch from  $-0.50$  to  $1.05$  V—curve 1; in the potential switch from  $-0.50$  to  $1.50$  V—curve 2) ( $\text{CH}_3\text{CN}$ ,  $C = 4$  mM,  $0.15$  M TBAP, scan rate  $200$   $\text{mV}\cdot\text{s}^{-1}$ ).

A significant difference of the electrochemical behavior of **2** in acetonitrile from the electrochemical picture of **2** in dichloromethane is the absence of a separation of the second and third stages of oxidation: There is one two-electron oxidation peak. Complex **2** in acetonitrile exhibits a behavior similar to **1** in dichloromethane: Both redox active fragments of the ligand are involved in the second stage of oxidation, namely the *o*-semiquinone ligand is converted to *o*-benzoquinone, and the phenolic group is oxidized to the radical cation.

The synthesized ligands (as well as the complexes based on them) contain several electroactive centers. Complexes **1** and **2** significantly expand their redox capabilities owing to the fact that they can act as: (1) electron donors due to the catecholate metallocycle capable of sequential oxidations, and (2) donors of the hydrogen atoms forming a stable phenoxyl radical. This ability of ligands can be used in catalysis in coordination with transition metal ions.

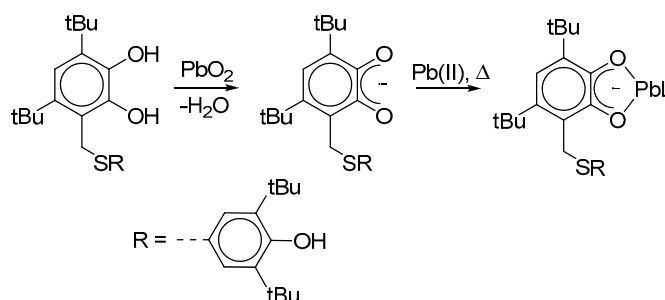
In contrast to the previously studied triphenylantimony(V) catecholato complexes with additional redox centers (ferrocenyl, morpholine, piperazine groups [18,24,30]), whose electrochemical activation

is observed at potentials shifted to the cathode region as compared to the “catechol/*o*-semiquinone” transition, compounds **1** and **2** are characterized by electrooxidation of the phenolic fragment at potentials that are close to the second redox transition “*o*-semiquinone/*o*-benzoquinone”. This fact indicates the convergence of the boundary redox orbitals of the phenolic and *o*-semiquinone fragments in the electro-generated monocationic complexes.

#### 2.4. EPR Experiments

The oxidation of the catechol thioether **L**<sub>1</sub> with lead dioxide in toluene proceeds slowly. In this case, immediately after mixing the reagents, a superposition of two doublets was observed (Figure S14(1)). One of the doublets has the following parameters:  $g_i = 2.0020$ ,  $a_i(^1\text{H}) = 3.6$  G, the second:  $g_i = 2.0009$ ,  $a_i(^1\text{H}) = 3.85$  G. The intensive stirring and heating of the reaction mixture leads to an increase in the intensity of the EPR spectrum, and the intensity of the second doublet grows significantly more noticeably in comparison with the intensity of the first doublet (Figure S14(2)). An increase in the signal intensity allows one to see the satellite splitting of the second signal on magnetic isotopes of lead (<sup>207</sup>Pb,  $I = 1/2$ , 22.1% [93]) with the hyper-fine structure (HFS) constant  $a_i(^{207}\text{Pb}) = 70.5$  G. The doublet with satellite splitting was simulated using the WinEPR SimFonia 1.25 program, and the simulation spectrum is shown in Figure S14(3).

It can be concluded that the interaction of catechol **L**<sub>1</sub> with lead dioxide slowly leads to the deprotonation of catechol with the formation of the *o*-semiquinone radical anion at the first stage (Scheme 8), which has a doublet with parameters  $g_i = 2.0020$ ,  $a_i(^1\text{H}) = 3.6$  G without any satellite splitting on the lead isotopes.



**Scheme 8.** The oxidation of catechol **L**<sub>1</sub> with lead(IV) oxide.

The process accelerates when the mixture is heated; however, the formation of *o*-semiquinone complex with lead(II) occurs, the EPR spectrum of which increases in intensity with the heating of the sample (the second EPR spectrum).

The oxidation of catechol **L**<sub>2</sub> with lead dioxide in a toluene solution proceeds more easily than the oxidation of **L**<sub>1</sub> and does not require heating. In this case, initially (Figure 9(1)), a wide doublet appears with the parameters  $g_i = 1.9967$ ,  $a_i(^1\text{H}) = 2.3$  G, which disappears gradually with further stirring of the reaction mixture (Figure 9(2)) with the simultaneous appearance of a triplet with some other parameters ( $g_i = 2.0050$ ,  $a_i(^1\text{H}) = 1.1$  G). Twenty minutes after the beginning reaction, only one triplet signal is observed practically (Figure 9(3)). Both spectra were simulated using WinEPR SimFonia 1.25. Simulations of the triplet and doublet spectra are shown in Figure 9(4),(5), respectively.

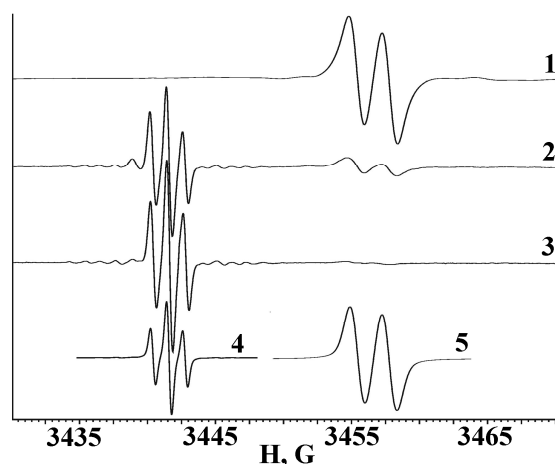
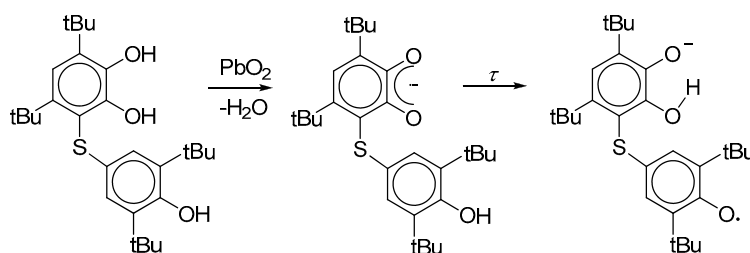


**Figure 9.** The X-band EPR spectrum of the mixture “L<sub>2</sub> + PbO<sub>2</sub>” in toluene immediately after mixing the reagents (spectrum 1), after stirring for 10 min (spectrum 2), and after stirring for 20 min (spectrum 3); Simulated EPR spectra (WinEPR SimFonia 1.25): triplet with parameters  $g_i = 2.0050$ ,  $a_i(^2\text{H}) = 1.1$  G (spectrum 4), doublet with parameters  $g_i = 1.9967$ ,  $a_i(^1\text{H}) = 2.3$  G (spectrum 5).

The oxidation of L<sub>2</sub> with lead dioxide proceeds with the deprotonation of catechol with the formation of the *o*-semiquinone radical (Scheme 9), and the doublet signal from this radical is recorded at the initial time. However, a decrease in the intensity of this signal and an increase in the intensity of the triplet with the HFS constant on two equivalent protons of 1.1 G characteristic of 4,6-di-*tert*-butylphenoxy radicals gradually occurs. Thus, we can conclude that either the *o*-semiquinone formed at the initial stage oxidizes and deprotonates the phenolic group to form a phenoxy radical during the reaction, or (since the reaction with lead dioxide is heterogeneous, requiring an excess of oxidizing agent) during the reaction, oxidation of the 4,6-di-*tert*-butylphenol group in the catechol proceeds more slowly than the oxidation of the catechol fragment, and at a certain moment, the concentration of the *o*-semiquinone radical begins to decrease with a simultaneous increase in the concentration of the phenoxy radical.

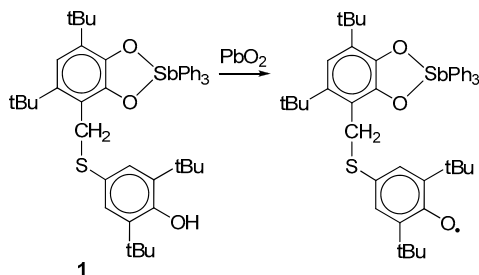


**Scheme 9.** The oxidation of L<sub>2</sub> with lead(IV) oxide.

Earlier, it was shown that thioether L<sub>3</sub> is oxidized by lead(IV) oxide in toluene solution with the formation of lead *o*-semiquinonato derivatives [14a]. In the EPR spectrum, a doublet at  $g_i = 2.0004$  with satellite splitting, typical for lead(II) *o*-semiquinolates, was observed. This fact is also explained by the initial formation of the *o*-semiquinone radical anion further coordinated to metal. The hyperfine structure of the EPR spectrum of a system “L<sub>3</sub>+PbO<sub>2</sub>” is caused by hyperfine splitting of a signal on the one proton nucleus in the fifth position of the *o*-semiquinone six-membered carbon ring with a satellite splitting on the magnetic lead isotope (<sup>207</sup>Pb, 22.1%,  $I = 1/2$ ):  $a_i(^1\text{H}) = 2.65$  G,  $a_i(^{207}\text{Pb}) = 22.75$  G [48].

The oxidation of triphenylantimony(V) catecholate 1 with lead(IV) oxide in toluene proceeds with weak heating (to 50°C) and leads to the formation of the corresponding phenoxy radical (Scheme 10) with an isotropic multiplet EPR spectrum (Figure 10) with  $g_i = 2.0050$ . The spectrum was simulated with Easyspin 5.2.25 [94], and the following HFS constants were revealed: the hyperfine coupling with

two aromatic protons in meta-positions to the oxy group with  $a_i(2\ ^1\text{H}) = 0.89\ \text{G}$ , and coupling with two non-equivalent protons of the S-CH<sub>2</sub> group in the para-position of the phenoxy ring with  $a_i(1\ ^1\text{H}) = 1.97\ \text{G}$  and  $a_i(1\ ^1\text{H}) = 3.30\ \text{G}$ . The nonequivalence of these methylene protons is caused by their different positions towards the pi-system of the phenoxy radical.



**Scheme 10.** The oxidation of complex **1** with PbO<sub>2</sub> with formation of the phenoxy radical.

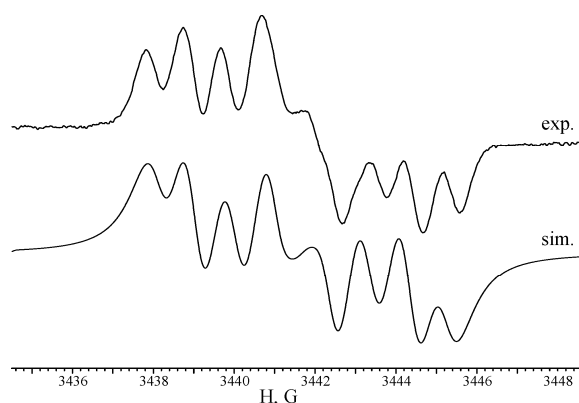


**Figure 10.** The X-band EPR spectrum of a mixture “1+PbO<sub>2</sub>”: exp.—the experimental spectrum (toluene, 298 K); sim.—its simulation (WinEPR SimFonia 1.25).

The EPR data of experiments on the oxidation of free ligands indicate the tendency of **L**<sub>1</sub> and **L**<sub>2</sub> to form *o*-semiquinone radical anions. The difference is the great propensity of **L**<sub>1</sub> to form stable chelate rings, while for **L**<sub>2</sub> the subsequent generation of a stable phenoxy radical is possible. Complex **1** in reaction with lead(IV) oxide tends to form a phenoxy radical, which is consistent with the possibility of simultaneous activation of the catechol cycle and the phenolic group during electrooxidation in a polar solvent (MeCN).

### 3. Materials and Methods

#### 3.1. General Remarks

All the experiments on the synthesis and study of properties of complexes were carried out in evacuated ampoules in the absence of oxygen and water. The solvents used were purified and dried by standard methods [95]. The infrared spectra of the complexes in the 4000–400 cm<sup>−1</sup> range were recorded on an FSM 1201 Fourier-IR spectrometer in nujol mull. The NMR spectra of **L**<sub>1</sub> and **L**<sub>2</sub> were recorded in CDCl<sub>3</sub> solution using a “Bruker DPX 200” instrument (200 MHz for <sup>1</sup>H, and ~50 MHz for <sup>13</sup>C), and the NMR spectra of **1** and **2** were recorded in CDCl<sub>3</sub> solution using a “Bruker ARX 400” instrument (400 MHz for <sup>1</sup>H, and ~100 MHz for <sup>13</sup>C), with Me<sub>4</sub>Si as the internal standard. The C, H, S elemental analysis was performed on an Elemental Analyzer “Elementar vario EL Cube”; the antimony content was accomplished by combustion analysis.



### 3.2. Cyclic Voltammetry

The electrochemical studies were carried out using IPC-Pro potentiostat in three-electrode mode. The stationary glassy carbon ( $d = 2$  mm) disk was used as the working electrode; the auxiliary electrode was a platinum-flag electrode. The reference electrode was Ag/AgCl/KCl(sat.) with a watertight diaphragm. All measurements were carried out under argon. The samples were dissolved in the pre-deaerated solvent. The rate scan was  $0.2 \text{ Vs}^{-1}$ . The supporting electrolyte  $0.15 \text{ M} [\text{Bu}_4\text{N}]\text{ClO}_4$  (99%, «Acros») underwent recrystallization twice from aqueous EtOH and then it was dried in vacuum (48 h) under  $50^\circ\text{C}$ . The concentration of the compounds was  $1.5\text{--}4.0 \text{ mM}$ .

### 3.3. X-Ray Diffraction Studies

The X-ray diffraction data were collected on a SMART APEX I ( $\text{L}_1$ , **1**) diffractometer (graphite monochromated,  $\text{MoK}\alpha$ -radiation,  $\omega$ -scan technique,  $\lambda = 0.71073 \text{ \AA}$ ) at  $100 \text{ K}$ . The intensity data were integrated by the SAINT program [96]. SADABS [97] was used to perform area-detector scaling and absorption corrections. The structures were solved by direct methods and were refined on  $F^2$  using the SHELXTL package [98]. All non-hydrogen atoms were refined anisotropically. All hydrogen atoms were placed in geometrically idealized positions and treated as riding with  $U_{\text{iso}}(\text{H}) = 1.2 \text{ Ueq}$  ( $U_{\text{iso}}(\text{H}) = 1.5 \text{ Ueq}$  for the hydrogen atoms in  $\text{CH}_3$  groups) of their parent atoms. Crystal data and details of the data collection and structure refinement for  $\text{L}_1$  and **1** are given in Table S1. The selected bond lengths for  $\text{L}_1$  are listed in Table S2, and the selected bond angles for **1** are in Table S3 of ESI. The structure parameters were deposited with the Cambridge Structural Database (CCDC 1978538 ( $\text{L}_1$ ) and 1978539 (**1**); deposit@ccdc.cam.ac.uk or [http://www.ccdc.cam.ac.uk/data\\_request/cif](http://www.ccdc.cam.ac.uk/data_request/cif)).

### 3.4. Synthesis of Catechol Thioethers

3,5-Di-*tert*-butyl-6-methoxymethylcatechol and 4,6-di-*tert*-butyl-3-(4-hydroxyphenylthio)catechol ( $\text{L}_3$ ) were synthesized according to previous reports [8c,14a].

#### 3.4.1. 4,6-Di-*tert*-butyl-3-(3,5-di-*tert*-butyl-4-hydroxyphenyl-thiomethyl)catechol $\text{L}_1$

Ligand was prepared according the next procedure: 3,5-di-*tert*-butyl-6-methoxymethylcatechol ( $1.5 \text{ mmol}$ ,  $0.400 \text{ g}$ ) and 2,6-di-*tert*-butyl-4-mercaptophenol ( $1.5 \text{ mmol}$ ,  $0.357 \text{ g}$ ) were dissolved in acetic acid ( $15 \text{ mL}$ ) under argon atmosphere, then the mixture was heated for  $12 \text{ h}$  at  $60^\circ\text{C}$ . Further water ( $25 \text{ mL}$ ) was added to the reaction mixture and a precipitate was filtrated. The product was dried under vacuum, then it was recrystallized from *n*-hexane to form white crystals. The yield was  $0.37 \text{ g}$  (52%). M.p.  $174\text{--}176^\circ\text{C}$ . Anal. calc. for  $\text{C}_{29}\text{H}_{44}\text{O}_3\text{S}$  (%): C, 73.68; H, 9.38; S, 6.78; found: C, 73.54; H, 9.42; S, 6.70.  $^1\text{H NMR}$  ( $200 \text{ MHz}$ ,  $\text{CDCl}_3$ ,  $\delta$ , ppm): 1.22 (s., 9 H, tBu, Cat), 1.37 (s., 18 H, tBu, Phenol), 1.42 (s., 9 H, tBu, Cat), 4.35 (s., 2 H,  $\text{CH}_2\text{-S}$ ), 5.30 (s., 1 H, OH), 6.12 (s., 1 H, OH), 6.89 (s., 1 H, arom.  $\text{C}_6\text{H}_1$ ), 7.18 (s., 2 H, arom.  $\text{C}_6\text{H}_2$ ), 7.26 (s., 1 H, OH).  $^{13}\text{C}\{^1\text{H}\}$  NMR ( $50 \text{ MHz}$ ,  $\text{CDCl}_3$ ,  $\delta$ , ppm): 29.48, 30.07, 31.99, 34.27, 34.93, 35.43, 36.40, 116.73, 119.28, 121.59, 130.95, 133.64, 136.78, 138.71, 142.91, 143.34, 154.59. FT-IR (KBr):  $\nu = 3629, 3510, 3198, 3057, 2955, 2910, 2870, 1481, 1425, 1370, 1290, 1235, 1144 \text{ cm}^{-1}$ .

#### 3.4.2. 4,6-Di-*tert*-butyl-3-(3,5-di-*tert*-butyl-4-hydroxyphenyl-thio)catechol $\text{L}_2$

This ligand was prepared according to the followed protocol. 2,6-Di-*tert*-butyl-4-mercaptophenol ( $1 \text{ mmol}$ ,  $0.238 \text{ g}$ ) in  $10 \text{ mL}$  ethanol was added dropwise to a solution of 3,5-di-*tert*-butyl-*o*-benzoquinone in  $20 \text{ mL}$  of ethanol ( $0.5 \text{ mmol}$ ,  $0.110 \text{ g}$ ) over a period of  $2\text{--}3 \text{ h}$  and the mixture was stirred under argon till decoloration of the reaction media at room temperature. The volume was concentrated under a reduced pressure to yield a crude solid. The product was recrystallized from dry ethanol, dried under vacuum, and isolated as yellow powder. The yield was  $0.08 \text{ g}$  (35%). M.p.  $165\text{--}167^\circ\text{C}$ . Anal. calc. for  $\text{C}_{28}\text{H}_{42}\text{O}_3\text{S}$  (%): C, 73.32; H, 9.23; S, 6.99; found: C, 73.48; H, 9.26; S, 6.87.  $^1\text{H NMR}$  ( $200 \text{ MHz}$ ,  $\text{CDCl}_3$ ,  $\delta$ , ppm): 1.25 (s., 18H, tBu), 1.31 (s., 9H, tBu), 1.41 (s., 9H, tBu), 4.93 (s., 1H, OH), 6.87 (s., 1H,  $\text{C}_6\text{H}_1$ ), 6.91 (s., 2H,  $\text{C}_6\text{H}_2$ ).  $^{13}\text{C}\{^1\text{H}\}$  NMR ( $50 \text{ MHz}$ ,  $\text{CDCl}_3$ ,  $\delta$ , ppm): 29.35, 29.63, 34.90, 34.98, 35.02, 118.05, 119.13,

127.73, 134.06, 136.00, 136.29, 138.40, 143.23, 146.14. FT-IR (KBr):  $\nu = 3629, 3485, 2958, 2908, 2868, 1644, 1663, 1485, 1458, 1392, 1363, 1218, 1164 \text{ cm}^{-1}$ .

### 3.5. Synthesis of Complexes

#### 3.5.1. Complex (6-(CH<sub>2</sub>-S-tBu<sub>2</sub>Phenol)-3,5-DBCat)SbPh<sub>3</sub> (**1**)

A solution of 4,6-di-*tert*-butyl-3-(3,5-di-*tert*-butyl-4-hydroxyphenyl-thiomethyl)catechol **L**<sub>1</sub> (0.236 g, 0.5 mmol) in 25 mL of toluene was added with stirring to a toluene solution of triphenylantimony dibromide (0.256 g, 0.5 mmol, 10–15 mL of toluene) under argon atmosphere. Then two equivalents of the triethylamine (0.14 mL, 1 mmol) were added to the toluene solution. After the addition of reagents and changing the color of the solution by yellow to orange, the reaction mixture was stirred for 2 h. The formed white precipitate of triethylammonium bromide was filtered off. The volume of filtrate was concentrated under a reduced pressure to a half volume and stored at  $-18^\circ\text{C}$  for five days. The X-ray-suitable yellow crystals of **1** were collected by decantation, and dried under vacuum. The yield was 0.300 g (73%). Anal. calc. for C<sub>47</sub>H<sub>57</sub>O<sub>3</sub>SSb (%): C, 68.53; H, 6.97; S, 3.89; Sb, 14.78. Found (%): C, 68.62; H, 7.05; S, 4.01; Sb, 14.53. <sup>1</sup>H NMR (400 MHz,  $\delta$ , ppm): 1.40 (s, 18H, tBu), 1.41 (s, 9H, tBu), 1.42 (s, 9H, tBu), 4.55 (s, 2H, CH<sub>2</sub>S), 5.18 (s, 1H, OH), 6.70 (s, 1H, arom. C<sub>6</sub>H<sub>1</sub>), 7.36 (s, 2H, arom. C<sub>6</sub>H<sub>2</sub>), 7.40–7.50 (m, 9H, Ph), 7.87–7.91 (m, 6H, Ph). <sup>13</sup>C{<sup>1</sup>H} NMR (100 MHz,  $\delta$ , ppm): 29.63, 30.19, 32.43, 34.36, 34.65, 35.85, 36.48, 112.61, 117.58, 127.81, 128.75, 129.06, 131.02, 131.66, 135.44, 136.27, 136.75, 137.81, 142.56, 147.52, 152.86. FT-IR (KBr):  $\nu = 3541, 3068, 3045, 2957, 2910, 2873, 1580, 1480, 1431, 1394, 1360, 1258, 1240, 1168 \text{ cm}^{-1}$ .

#### 3.5.2. Complex (6-(S-Phenol)-3,5-DBCat)SbPh<sub>3</sub> (**2**)

A solution of the 4,6-di-*tert*-butyl-3-(4-hydroxyphenylthio)catechol (0.173 g, 0.5 mmol) in 20 mL of toluene was added dropwise with stirring to a toluene solution of triphenylantimony dibromide (0.256 g, 0.5 mmol, 10–15 mL of toluene) under argon atmosphere. Then two equivalents of the triethylamine (0.14 mL, 1 mmol) were added to toluene solution. After the addition of reagents and changing the color of the solution to pale yellow, the reaction mixture was stirred for 2 h. The formed white precipitate of ammonium salt was filtered off. The volume was concentrated under a reduced pressure to yield a yellow crude solid. The product was recrystallized from a mixture of the solvents pentane and hexane (v/v = 1/1), dried under vacuum, and isolated as a yellow powder of **2**. The yield was 0.175 g (50%). Anal. calc. for C<sub>38</sub>H<sub>39</sub>O<sub>3</sub>SSb (%): C, 65.43; H, 5.64; S, 4.60; Sb, 17.46. Found (%): C, 65.30; H, 5.72; S, 4.55; Sb, 17.60. <sup>1</sup>H NMR (400 MHz,  $\delta$ , ppm): 1.45 (s, 9H, tBu), 1.51 (s, 9H, tBu), 4.51 (br.s, 1H, OH), 6.51 (d.m, J = 8.7 Hz, 2H, C<sub>6</sub>H<sub>4</sub>), 6.82 (s, 1H, Ar), 6.94 (d.m, J = 8.7 Hz, 2H, C<sub>6</sub>H<sub>4</sub>), 7.35–7.41 (m, 6H, Ar), 7.43–7.48 (m, 3H, Ar), 7.51–7.56 (m, 6H, Ar). <sup>13</sup>C{<sup>1</sup>H} NMR (100 MHz,  $\delta$ , ppm): 29.53, 31.46, 34.80, 36.69, 112.63, 113.01, 115.48, 127.64, 129.03, 131.00, 131.34, 133.45, 135.10, 137.32, 141.25, 143.19, 149.86, 152.48. FT-IR (KBr):  $\nu = 3411, 3056, 2958, 2910, 2870, 1490, 1431, 1397, 1257, 1238, 1167 \text{ cm}^{-1}$ .

## 4. Conclusions

Thus, in this work, new polyfunctional sterically hindered catechols with an additional phenolic group connected by a bridging sulfur atom, as well as triphenylantimony(V) catecholates based on these ligands, were synthesized. The molecular structures of free ligand **L**<sub>1</sub> and complex **1** in the crystal state were determined by single-crystal X-ray analysis. The electrochemical investigations have shown that the electrooxidation of ligands in the first stage leads to the formation of the corresponding *o*-benzoquinones. The second anode stage involves the oxidation of the phenolic moiety. The results of the EPR studies confirmed the primary oxidation of the catechol group with the formation of the *o*-semiquinone radical anion. The electrooxidation of complexes **1** and **2** in dichloromethane is somewhat different from each other. For compound **2**, the three oxidation stages are clearly fixed, the first two stages correspond to the conversion of the catecholate form of the ligand to *o*-benzosemiquinone

and then to *o*-benzoquinone, and the third peak characterizes the oxidation of the phenolic fragment. For complex **1**, the first redox stage also affects the catecholate group, and the second redox process can involve both *o*-semiquinone and phenolic fragments in this electrode process.

In the coordinating solvent (acetonitrile), the electrochemical behavior of compound **2** becomes identical to that one for complex **1** in dichloromethane. At the same time, in acetonitrile for complex **1**, the current of the first anode peak increases significantly, which implies two-electron oxidation leading to a dication containing the one-electron oxidized form of the catecholate ligand and phenoxy radical. The oxidation of complex **1** in toluene with lead dioxide leads to the fixation of the phenoxy radical. This indicates the possibility of activation of the phenolic group during electrooxidation. The combination of electrochemical and spectral data indicates the convergence of the boundary redox orbitals of the phenolic and *o*-semiquinone fragments in the electro-generated monocationic triphenylantimony(V) complexes.

**Supplementary Materials:** The following are available online at <http://www.mdpi.com/1420-3049/25/8/1770/s1>, Figures S1–S8: The NMR spectra of compounds, Table S1: Crystal data and structure refinement for L1 and 1, Table S2: The selected bond lengths for L1, Table S3: The selected bond lengths for 1, Figure S9: The intermolecular hydrogen bonds in crystals of L1, Figure S10: The order of complex 1 molecules in crystal cell with the indication of intermolecular hydrogen bonding, Figure S11: The CVs of compound L1 (CH<sub>2</sub>Cl<sub>2</sub>), Figure S12: the CV of the electrolysis products of compound L1, Figure S13: The CVs of compound 1 (CH<sub>3</sub>CN), Figure S14: The X-band EPR spectrum of the mixture “L1 + PbO<sub>2</sub>”. CCDC 1978538 (L1) and 1978539 (1) contain the supplementary crystallographic data for this paper. These data can be obtained free of charge from The Cambridge Crystallographic Data Centre via [www.ccdc.cam.ac.uk/data\\_request/cif](http://www.ccdc.cam.ac.uk/data_request/cif).

**Author Contributions:** Methodology, I.V.S.; resources and synthesis of precursors, M.V.A. and S.A.S.; synthesis of ligands, S.A.S.; synthesis of complexes, I.V.S. and A.I.P.; NMR and EPR investigations, A.I.P.; cyclic voltammetry, S.A.S. and I.V.S.; X-ray analysis, G.K.F.; supervision and project administration, N.T.B.; writing—original draft preparation, review and editing, I.V.S., M.V.A. and A.I.P.; funding acquisition, I.V.S., A.I.P. and N.T.B. All authors have read and agreed to the published version of the manuscript.

**Funding:** The reported study was funded by Russian Foundation for Basic Researches, project number 19-29-08003 mk. The spectroscopic and X-ray structural investigations of compounds were performed in the accordance with state assignment of IOMC RAS.

**Acknowledgments:** The spectroscopic and X-ray structural investigations of compounds were performed using the equipment of the analytical center of IOMC RAS.

**Conflicts of Interest:** The authors declare no conflict of interest.

## References

1. Pierpont, C.G.; Buchanan, R.M. Transition metal complexes of *o*-benzoquinone, *o*-semiquinone, and catecholate ligands. *Coord. Chem. Rev.* **1981**, *38*, 45–83. [[CrossRef](#)]
2. Mederos, A.; Dominguez, S.; Hernandez-Molina, R.; Sanchiz, J.; Brito, F. Coordinating ability of phenylenediamines. *Coord. Chem. Rev.* **1999**, *193*, 913–939. [[CrossRef](#)]
3. Pierpont, C.G. Studies on charge distribution and valence tautomerism in transition metal complexes of catecholate and semiquinonate ligands. *Coord. Chem. Rev.* **2001**, *216*, 99–125. [[CrossRef](#)]
4. Pierpont, C.G. Unique properties of transition metal quinone complexes of the MQ<sub>3</sub> series. *Coord. Chem. Rev.* **2001**, *219*, 415–433. [[CrossRef](#)]
5. Zanello, P.; Corsini, M. Homoleptic, mononuclear transition metal complexes of 1,2-dioxolenes: Updating their electrochemical-to-structural (X-ray) properties. *Coord. Chem. Rev.* **2006**, *250*, 2000–2022. [[CrossRef](#)]
6. Poddel'sky, A.I.; Cherkasov, V.K.; Abakumov, G.A. Transition metal complexes with bulky 4,6-di-tert-butyl-N-aryl(alkyl)-*o*-iminobenzoquinonato ligands: Structure, EPR and magnetism. *Coord. Chem. Rev.* **2009**, *253*, 291–324. [[CrossRef](#)]
7. Kaim, W.; Schwederski, B. Non-innocent ligands in bioinorganic chemistry—An overview. *Coord. Chem. Rev.* **2010**, *254*, 1580–1588. [[CrossRef](#)]
8. Kaim, W. The shrinking world of innocent ligands: Conventional and non-conventional redox-active ligands. *Eur. J. Inorg. Chem.* **2012**, *2012*, 343–348. [[CrossRef](#)]
9. Kaim, W.; Paretzki, A. Interacting metal and ligand based open shell systems: Challenges for experiment and theory. *Coord. Chem. Rev.* **2017**, *344*, 345–354. [[CrossRef](#)]

10. Kaim, W.; Beyer, K.; Filippou, V.; Záliš, S. Charge and spin coupling in copper compounds with hemilabile noninnocent ligands—Ambivalence in three dimensions. *Coord. Chem. Rev.* **2018**, *355*, 173–179. [[CrossRef](#)]
11. Kaim, W.; Das, A.; Fiedler, J.; Záliš, S.; Sarkar, B. NO and NO<sub>2</sub> as non-innocent ligands: A comparison. *Coord. Chem. Rev.* **2020**, *404*, 213114. [[CrossRef](#)]
12. Piskunov, A.V.; Chegerev, M.G.; Fukin, G.K. Redox-induced C–C bond formation reaction between mono-*o*-amidophenolate tin complexes and allylhalides. *J. Organometal. Chem.* **2016**, *803*, 51–57. [[CrossRef](#)]
13. Chegerev, M.G.; Piskunov, A.V.; Maleeva, A.V.; Fukin, G.K.; Abakumov, G.A. Multiple Reactivity of Sn<sup>II</sup> Complexes Bearing Catecholate and *o*-Amidophenolate Ligands. *Eur. J. Inorg. Chem.* **2016**, 3813–3821. [[CrossRef](#)]
14. Chegerev, M.G.; Piskunov, A.V.; Starikova, A.A.; Kubrin, S.P.; Fukin, G.K.; Cherkasov, V.K.; Abakumov, G.A. Redox Isomerism in Main-Group Chemistry: Tin Complex with *o*-Iminoquinone Ligands. *Eur. J. Inorg. Chem.* **2018**, *2018*, 1087–1092. [[CrossRef](#)]
15. Abakumov, G.A.; Poddel'sky, A.I.; Grunova, E.V.; Cherkasov, V.K.; Fukin, G.K.; Kurskii, Yu.A.; Abakumova, L.G. Reversible Binding of Dioxygen by a Non-transition-Metal Complex. *Angew. Chem. Int. Ed.* **2005**, *44*, 2767–2771. [[CrossRef](#)]
16. Cherkasov, V.K.; Abakumov, G.A.; Grunova, E.V.; Poddel'sky, A.I.; Fukin, G.K.; Baranov, E.V.; Kurskii, Y.A.; Abakumova, L.G. Triphenylantimony(V) Catecholates and *o*-Amidophenolates: Reversible Binding of Molecular Oxygen. *Chem. Eur. J.* **2006**, *12*, 3916–3927. [[CrossRef](#)]
17. Poddel'sky, A.I.; Smolyaninov, I.V.; Kurskii, Yu.A.; Fukin, G.K.; Berberova, N.T.; Cherkasov, V.K.; Abakumov, G.A. New morpholine- and piperazine-functionalised triphenylantimony(V) catecholates: The spectroscopic and electrochemical studies. *J. Organometal. Chem.* **2010**, *695*, 1215–1224. [[CrossRef](#)]
18. Fukin, G.K.; Baranov, E.V.; Poddel'sky, A.I.; Cherkasov, V.K.; Abakumov, G.A. Reversible Binding of Molecular Oxygen to Catecholate and Amidophenolate Complexes of Sb<sup>V</sup>: Electronic and Steric Factors. *ChemPhysChem* **2012**, *13*, 3773–3776. [[CrossRef](#)]
19. Poddel'skii, A.I.; Okhlopkova, L.S.; Meshcheryakova, I.N.; Druzhkov, N.O.; Smolyaninov, I.V.; Fukin, G.K. Triphenylantimony(V) Catecholates Based on *o*-Quinones, Derivatives of Benzo[b][1,4]-Dioxines and Benzo[b][1,4]-Dioxepines. *Russ. J. Coord. Chem.* **2019**, *45*, 133–141. [[CrossRef](#)]
20. Ilyakina, E.V.; Poddel'sky, A.I.; Cherkasov, V.K.; Abakumov, G.A. Binding of NO by nontransition metal complexes. *Mendeleev Commun.* **2012**, *22*, 208–210. [[CrossRef](#)]
21. De Paiva, Y.G.; da Rocha Ferreira, F.; Silva, T.L.; Labbé, E.; Buriez, O.; Amatore, C.; Goulart, M.O.F. Electrochemically Driven Supramolecular Interaction of Quinones and Ferrocifens: An Example of Redox Activation of Bioactive Compounds. *Curr. Top. Med. Chem.* **2015**, *15*, 136–162. [[CrossRef](#)] [[PubMed](#)]
22. Amatore, C.; Labbe, E.; Buriez, O. Molecular electrochemistry: A central method to understand the metabolic activation of therapeutic agents. The example of metallocifen anti-cancer drug candidates. *Curr. Opin. Electrochem.* **2017**, *2*, 7–12. [[CrossRef](#)]
23. Lee, H.Z.S.; Chau, F.; Top, S.; Jaouen, G.; Vessieres, A.; Labbe, E.; Buriez, O. New mechanistic insights into osmium-based tamoxifen derivatives. *Electrochim. Acta* **2019**, *302*, 130–136. [[CrossRef](#)]
24. Smolyaninov, I.V.; Poddel'sky, A.I.; Baryshnikova, S.V.; Kuzmin, V.V.; Korchagina, E.O.; Arsenyev, M.V.; Smolyaninova, S.A.; Berberova, N.T. Electrochemical transformations and evaluation of antioxidant activity of some Schiff bases containing ferrocenyl and (thio-)phenol, catechol fragments. *Appl. Organometal. Chem.* **2018**, *32*, e4121. [[CrossRef](#)]
25. Wanke, R.; Benisvy, L.; Kuznetsov, M.L.; Guedes da Silva, M.F.C.; Pombeiro, A.J.L. Persistent Hydrogen-Bonded and Non-Hydrogen-Bonded Phenoxyl Radicals. *Chem. Eur. J.* **2011**, *17*, 11882–11892. [[CrossRef](#)]
26. Neidlinger, A.; Ksenofontov, V.; Heinze, K. Proton-Coupled Electron Transfer in Ferrocenium–Phenolate Radicals. *Organometallics* **2013**, *32*, 5955–5965. [[CrossRef](#)]
27. Neidlinger, A.; Forster, C.; Heinze, K. How Hydrogen Bonds Affect Reactivity and Intervalence Charge Transfer in Ferrocenium-Phenolate Radicals. *Eur. J. Inorg. Chem.* **2016**, *2016*, 1274–1286. [[CrossRef](#)]
28. Druzhkov, N.O.; Egorova, E.N.; Arsenyev, M.V.; Baranov, E.V.; Cherkasov, V.K. Functionalization of sterically hindered catechol and *o*-benzoquinone with 2,2,6,6-tetramethylpiperidine-1-oxyl. *Russ. Chem. Bull.* **2016**, *65*, 2855–2860. [[CrossRef](#)]

29. Egorova, E.N.; Druzhkov, N.O.; Kozhanov, K.A.; Cherkasov, A.V.; Cherkasov, V.K. Heterospin biradicals based on new piperidineoxyl-substituted 3,6-di-tert-butyl-o-benzoquinone. *Russ. Chem. Bull.* **2017**, *66*, 1629–1635. [[CrossRef](#)]
30. Baryshnikova, S.V.; Bellan, E.V.; Poddel'sky, A.I.; Arsenyev, M.V.; Smolyaninov, I.V.; Fukin, G.K.; Piskunov, A.V.; Berberova, N.T.; Cherkasov, V.K.; Abakumov, G.A. Tin(IV) and antimony(V) complexes bearing catecholate ligand connected to ferrocene. Synthesis, molecular structure and electrochemical properties. *Eur. J. Inorg. Chem.* **2016**, *2016*, 5230–5241. [[CrossRef](#)]
31. Poddel'sky, A.I.; Arsen'ev, M.V.; Okhlopko, L.S.; Smolyaninov, I.V.; Fukin, G.K. New Catecholate Complexes of Triphenylantimony(V) Based on 6-Iminomethyl-3,5-Di-tert-Butylpyrocatechols N-Functionalized by the Aniline or Phenol Group. *Russ. J. Coord. Chem.* **2017**, *43*, 843–851. [[CrossRef](#)]
32. Poddel'sky, A.I.; Druzhkov, N.O.; Fukin, G.K.; Cherkasov, V.K.; Abakumov, G.A. Bifunctional iminopyridino-catechol and its o-quinone: Synthesis and investigation of coordination abilities. *Polyhedron* **2017**, *124*, 41–50. [[CrossRef](#)]
33. Klementieva, S.V.; Kuropatov, V.A.; Fukin, G.K.; Romanenko, G.V.; Bogomyakov, A.S.; Cherkasov, V.K.; Abakumov, G.A. Mono- and Binuclear Dimethylthallium(III) Complexes with o-Benzoquinone-TTF-o-Benzoquinone Ligand; Synthesis, Spectroscopy and X-ray Study. *Z. Anorg. Allgem. Chem.* **2011**, *637*, 232–241. [[CrossRef](#)]
34. Poddel'sky, A.I.; Arsenyev, M.V.; Astaf'eva, T.V.; Chesnokov, S.A.; Fukin, G.K.; Abakumov, G.A. New sterically-hindered 6th-substituted 3,5-di-tert-butylcatechols/o-quinones with additional functional groups and their triphenylantimony(V) catecholates. *J. Organometal. Chem.* **2017**, *835*, 17–24. [[CrossRef](#)]
35. Arsenyev, M.V.; Astaf'eva, T.V.; Baranov, E.V.; Poddel'sky, A.I.; Chesnokov, S.A. New sterically-hindered bis-catechol, bis-o-quinone and its bis-triphenylantimony(V) bis-catecholate. 3,5-Di-tert-butyl-6-methoxymethylcatechol as alkylating agent. *Mendeleev Commun.* **2018**, *28*, 76–78. [[CrossRef](#)]
36. Pointillart, F.; Klementieva, S.; Kuropatov, V.; Le Gal, Y.; Golhen, S.; Cadot, O.; Cherkasov, V.; Ouahab, L. A single molecule magnet behaviour in a  $D_{3h}$  symmetry Dy(III) complex involving a quinone-tetrathiafulvalene-quinone bridge. *Chem. Commun.* **2012**, *48*, 714–716. [[CrossRef](#)]
37. Kuropatov, V.; Klementieva, S.; Fukin, G.; Mitin, A.; Ketkov, S.; Budnikova, Y.; Cherkasov, V.; Abakumov, G. Novel method for the synthesis of functionalized tetrathiafulvalenes, an acceptor-donor-acceptor molecule comprising of two o-quinone moieties linked by a TTF bridge. *Tetrahedron* **2010**, *66*, 7605–7611. [[CrossRef](#)]
38. Klement'eva, S.V.; Fukin, G.K.; Baranov, E.V.; Cherkasov, V.K.; Abakumov, G.A. Investigation of photochemical transformations of tetrathiafulvalene-bridged di-o-quinone. *High Energy Chem.* **2011**, *45*, 423–427. [[CrossRef](#)]
39. Kuropatov, V.A.; Klementieva, S.V.; Poddel'sky, A.I.; Cherkasov, V.K.; Abakumov, G.A. ESR study of paramagnetic derivatives of sterically hindered di-o-quinone with the tetrathiafulvalene bridge. *Russ. Chem. Bull., Int. Ed.* **2010**, *59*, 1698–1706. [[CrossRef](#)]
40. Cherkasov, V.K.; Abakumov, G.A.; Fukin, G.K.; Klementyeva, S.V.; Kuropatov, V.A. Sterically Hindered o-Quinone Annulated with Dithiete: A Molecule Comprising Diolate and Dithiolate Coordination Sites. *Chem. Eur. J.* **2012**, *18*, 13821–13827. [[CrossRef](#)]
41. Tesema, Y.T.; Pham, D.M.; Franz, K.J. Synthesis and Characterization of Copper(II) Complexes of Cysteinyldopa and Benzothiazine Model Ligands Related to Pheomelanin. *Inorg. Chem.* **2006**, *45*, 6102–6104. [[CrossRef](#)] [[PubMed](#)]
42. Tesema, Y.T.; Pham, D.M.; Franz, K.J. Counterions Influence Reactivity of Metal Ions with Cysteinyldopa Model Compounds. *Inorg. Chem.* **2008**, *47*, 1087–1095. [[CrossRef](#)] [[PubMed](#)]
43. Poneti, G.; Poggini, L.; Mannini, M.; Cortigiani, B.; Sorace, L.; Otero, E.; Sainctavit, P.; Magnani, A.; Sessolia, R.; Dei, A. Thermal and optical control of electronic states in a single layer of switchable paramagnetic molecules. *Chem. Sci.* **2015**, *6*, 2268–2274. [[CrossRef](#)] [[PubMed](#)]
44. Smolyaninov, I.V.; Pitikova, O.V.; Rychagova, E.S.; Korchagina, E.O.; Poddel'sky, A.I.; Smolyaninova, S.A.; Berberova, N.T. Synthesis and antioxidant activity of sterically hindered bis-pyrocatechol thioethers. *Russ. Chem. Bull.* **2016**, *65*, 2861–2867. [[CrossRef](#)]
45. Poneti, G.; Mannini, M.; Cortigiani, B.; Poggini, L.; Sorace, L.; Otero, E.; Sainctavit, P.; Sessoli, R.; Dei, A. Magnetic and Spectroscopic Investigation of Thermally and Optically Driven Valence Tautomerism in Thioether-Bridged Dinuclear Cobalt-Dioxolene Complexes. *Inorg. Chem.* **2013**, *52*, 11798–11805. [[CrossRef](#)]



46. Guardingo, M.; Bellido, E.; Miralles-Llumà, R.; Faraudo, J.; Sedó, J.; Tatay, S.; Verdaguer, A.; Busqué, F.; Ruiz-Molina, D. Bioinspired Catechol-Terminated Self-Assembled Monolayers with Enhanced Adhesion Properties. *Small* **2014**, *10*, 1594–1602. [[CrossRef](#)]
47. Mancebo-Aracil, J.; Casagualda, C.; Moreno-Villaécija, M.A.; Nador, F.; García-Pardo, J.; Franconetti-García, A.; Busqué, F.; Alibés, R.; Esplandiú, M.J.; Ruiz-Molina, D.; et al. Bioinspired Functional Catechol Derivatives Through Simple Thiol Conjugate Addition. *Chem. Eur. J.* **2019**, *25*, 12367–12379. [[CrossRef](#)]
48. Smolyaninov, I.; Pitikova, O.; Korchagina, E.; Poddel'sky, A.; Luzhnova, S.; Berberova, N. Electrochemical behavior and anti/prooxidant activity of thioethers with redox-active catechol moiety. *Monatsh. Chem.* **2018**, *149*, 1813–1826. [[CrossRef](#)]
49. Smolyaninov, I.V.; Pitikova, O.V.; Poddel'sky, A.I.; Berberova, N.T. Electrochemical transformations and antiradical activity of asymmetrical RS-substituted pyrocatechols. *Russ. Chem. Bull.* **2018**, *67*, 1857–1867. [[CrossRef](#)]
50. Smolyaninov, I.V.; Pitikova, O.V.; Korchagina, E.O.; Poddel'sky, A.I.; Fukin, G.K.; Luzhnova, S.A.; Tichkomirov, A.M.; Ponomareva, E.N.; Berberova, N.T. Bifunctional catechol thioethers with physiologically active fragments: Electrochemistry, antioxidant and cryoprotective activities. *Bioorg. Chem.* **2019**, *89*, 103003. [[CrossRef](#)]
51. Loginova, N.V.; Koval'chuk, T.V.; Faletrov, Y.V.; Halauko, Y.S.; Osipovich, N.P.; Polozov, G.I.; Zheldakova, R.A.; Gres, A.T.; Halauko, A.S.; Azarko, I.I.; et al. Redox-active metal(II) complexes of sterically hindered phenolic ligands: Antibacterial activity and reduction of cytochrome *c*. Part II. Metal(II) complexes of *o*-diphenol derivatives of thioglycolic acid. *Polyhedron* **2011**, *30*, 2581–2591. [[CrossRef](#)]
52. Loginova, N.V.; Koval'chuk, T.V.; Polozov, G.I.; Osipovich, N.P.; Rytik, P.G.; Kucherov, I.I.; Chernyavskaya, A.A.; Sorokin, V.L.; Shadyro, O.I. Synthesis, characterization, antifungal and anti-HIV activities of metal(II) complexes of 4,6-di-*tert*-butyl-3-[(2-hydroxyethyl)thio]benzene-1,2-diol. *Eur. J. Med. Chem.* **2008**, *43*, 1536–1542. [[CrossRef](#)] [[PubMed](#)]
53. Do Prado, B.R.; Islam, A.; Frezard, F.; Demicheli, C. Chapter 10. Organometallic Compounds in Chemotherapy Against Leishmania. In *Drug Discovery for Leishmaniasis*; Rivas, L., Gil, C., Eds.; Royal Society of Chemistry: Cambridge, UK, 2017; pp. 199–223. [[CrossRef](#)]
54. Hadjikakou, S.K.; Ozturk, I.I.; Banti, C.N.; Kourkoumelis, N.; Hadjiliadis, N. Recent advances on antimony(III/V) compounds with potential activity against tumor cells. *J. Inorg. Biochem.* **2015**, *153*, 293–305. [[CrossRef](#)] [[PubMed](#)]
55. Islam, A.; Rodrigues, B.L.; Marzan, I.M.; Perreira-Maia, E.C.; Dittz, D.; Lopes, M.T.P.; Ishfaq, M.; Frezard, F.; Demichel, C. Cytotoxicity and apoptotic activity of novel organobismuth(V) and organoantimony(V) complexes in different cancer cell lines. *Eur. J. Med. Chem.* **2016**, *109*, 254–267. [[CrossRef](#)] [[PubMed](#)]
56. Christianson, A.M.; Gabbai, F.P. Antimony- and Bismuth-Based Materials and Applications. In *Main Group Strategies Towards Functional Hybrid Materials*; Baumgartner, T., Jäkle, F., Eds.; John Wiley & Sons: Chichester, UK, 2018; pp. 405–432. [[CrossRef](#)]
57. Hirai, M.; Gabbai, F.P. Squeezing fluoride out of water with a neutral bidentate antimony (V) Lewis acid. *Angew. Chem. Int. Ed.* **2015**, *54*, 1205–1209. [[CrossRef](#)]
58. Hirai, M.; Gabbai, F.P. Lewis acidic stiborafluorenes for the fluorescence turn-on sensing of fluoride in drinking water at ppm concentrations. *Chem. Sci.* **2014**, *5*, 1886–1893. [[CrossRef](#)]
59. Chen, C.-H.; Gabbai, F.P. Fluoride Anion Complexation by a Triptycene-Based Distiborane: Taking Advantage of a Weak but Observable C–H...F Interaction. *Angew. Chem. Int. Ed.* **2017**, *56*, 1799–1804. [[CrossRef](#)]
60. Arsenyev, M.V.; Shurygina, M.P.; Poddel'sky, A.I.; Druzhkov, N.O.; Chesnokov, S.A.; Fukin, G.K.; Cherkasov, V.K.; Abakumov, G.A. New poly-*o*-quinone-methacrylate and its dioxygen-active antimony-containing polymer. *J. Polym. Res.* **2013**, *20*, 98. [[CrossRef](#)]
61. Lenshina, N.A.; Shurygina, M.P.; Arsenyev, M.V.; Poddel'sky, A.I.; Zaitsev, S.D.; Chesnokov, S.A.; Abakumov, G.A. Optically controlled distribution of *o*-quinonemethacrylate metal complexes in polymer material. *J. Coord. Chem.* **2015**, *68*, 4159–4169. [[CrossRef](#)]
62. Chesnokov, S.A.; Lenshina, N.A.; Arsenyev, M.V.; Kovylin, R.S.; Baten'kin, M.A.; Poddel'sky, A.I.; Abakumov, G.A. Preparation of new dioxygen-active triphenylantimony(V) catecholate-containing porous polymer. *Appl. Organometal. Chem.* **2017**, *31*, e3553. [[CrossRef](#)]
63. Lide, D.R. (Ed.) *CRC Handbook of Chemistry and Physics*, 86th ed.; CRC Press: Boca Raton, FL, USA, 2005; 2544p.

64. Batsanov, S.S. The atomic radii of the elements. *Russ. J. Inorg. Chem.* **1991**, *36*, 1694–1706.
65. Brown, S.N. Metrical Oxidation States of 2-Amidophenoxide and Catecholate Ligands: Structural Signatures of Metal–Ligand  $\pi$  Bonding in Potentially Noninnocent Ligands. *Inorg. Chem.* **2012**, *51*, 1251–1260. [[CrossRef](#)] [[PubMed](#)]
66. Gai, K.; Fang, X.; Li, X.; Xu, J.; Wu, X.; Lin, A.; Yao, H. Synthesis of spiro[2.5]octa-4,7-dien-6-one with consecutive quaternary centers via 1,6-conjugate addition induced dearomatization of para-quinone methides. *Chem. Commun.* **2015**, *51*, 15831–15834. [[CrossRef](#)] [[PubMed](#)]
67. Jarava-Barrera, C.; Parra, A.; Lopez, A.; Cruz-Acosta, F.; Collado-Sanz, D.; Cardenas, D.J.; Tortosa, M. Copper-Catalyzed Borylative Aromatization of p-Quinone Methides: Enantioselective Synthesis of Dibenzyllic Boronates. *ACS Catal.* **2016**, *6*, 442–446. [[CrossRef](#)]
68. Santra, S.; Porey, A.; Jana, B.; Guin, J. N-Heterocyclic carbenes as chiral Brønsted base catalysts: A highly diastereo- and enantioselective 1,6-addition reaction. *Chem. Sci.* **2018**, *9*, 6446–6450. [[CrossRef](#)]
69. Hall, M.; Sowerby, D.B. Synthesis and crystal structure of bis(triphenylantimony catecholate) hydrate. A new square-pyramidal antimony(V) compound. *J. Am. Chem. Soc.* **1980**, *102*, 628–632. [[CrossRef](#)]
70. Holmes, R.R.; Day, R.O.; Chandrasekhar, V.; Holmes, J.M. Pentacoordinated molecules. 67. Formation and structure of cyclic five-coordinated antimony derivatives. The first square-pyramidal geometry for a bicyclic stiborane. *Inorg. Chem.* **1987**, *26*, 157–163. [[CrossRef](#)]
71. Tian, Z.; Tuck, D.G. Oxidation of elemental antimony by substituted ortho-benzoquinones. *J. Chem. Soc. Dalton Trans.* **1993**, 1381–1385. [[CrossRef](#)]
72. Gibbons, M.N.; Begley, M.J.; Blake, A.J.; Sowerby, D.B. New square-pyramidal organoantimony(V) compounds; crystal structures of (biphenyl-2,2'-diyl)phenylantimony(V) dibromide, dichloride and diisothiocyanate,  $\text{Sb}(2,2'\text{-C}_{12}\text{H}_8)\text{PhX}_2$  (X = Br, Cl or NCS), and of octahedral  $\text{SbPh}(\text{o-O}_2\text{C}_6\text{Cl}_4)\text{Cl}_2\text{-OEt}_2$ . *J. Chem. Soc. Dalton Trans.* **1997**, 2419–2425. [[CrossRef](#)]
73. Poddel'sky, A.I.; Piskunov, A.V.; Druzhkov, N.O.; Fukin, G.K.; Cherkasov, V.K.; Abakumov, G.A. New bis-o-benzoquinoid ligands with ethylene bridge and their metal complexes. Synthesis, Spectroscopy and X-ray study. *Z. Anorg. Allg. Chem.* **2009**, *635*, 2563–2571. [[CrossRef](#)]
74. Poddel'sky, A.I.; Smolyaninov, I.V.; Somov, N.V.; Berberova, N.T.; Cherkasov, V.K.; Abakumov, G.A. Antimony(V) catecholato complexes based on 5,5,8,8-tetramethyl-5,6,7,8-tetrahydronaphthalenequinone-2,3. Crystal structure of  $[\text{Ph}_4\text{Sb}]^+[\text{Ph}_2\text{Sb}(\text{Cat})_2]^-$ . *J. Organometal. Chem.* **2010**, *695*, 530–536. [[CrossRef](#)]
75. Poddel'sky, A.I.; Somov, N.V.; Druzhkov, N.O.; Cherkasov, V.K.; Abakumov, G.A. The binuclear trimethyl/triethylantimony(V) bis-catecholate derivatives of four-electron reduced 4,4'-di-(3-methyl-6-tert-butyl-o-benzoquinone). *J. Organometal. Chem.* **2011**, *696*, 517–522. [[CrossRef](#)]
76. Fukin, G.K.; Baranov, E.V.; Jelsch, C.; Guillot, B.; Poddelskii, A.I.; Cherkasov, V.K.; Abakumov, G.A. Experimental and Theoretical Investigation of Topological and Energetic Characteristics of Sb Complexes Reversibly Binding Molecular Oxygen. *J. Phys. Chem. A* **2011**, *115*, 8271–8281. [[CrossRef](#)] [[PubMed](#)]
77. Poddel'sky, A.I.; Baranov, E.V.; Fukin, G.K.; Cherkasov, V.K.; Abakumov, G.A. The nitro-substituted catecholates of triphenylantimony(V): Tetragonal-pyramidal vs. trigonal-bipyramidal coordination. *J. Organometal. Chem.* **2013**, *733*, 44–48. [[CrossRef](#)]
78. Arsen'ev, M.V.; Okhlopko, L.S.; Poddel'skii, A.I.; Fukin, G.K. Binuclear Triphenylantimony(V) Catecholate Based on Redox-Active Bis-o-Benzoquinone, a Bis-Catechol-Aldimine Derivative. *Russ. J. Coord. Chem.* **2018**, *44*, 162–168. [[CrossRef](#)]
79. Okhlopko, L.S.; Poddel'sky, A.I.; Smolyaninov, I.V.; Fukin, G.K.; Berberova, N.T.; Cherkasov, V.K.; Abakumov, G.A. Triphenylantimony(V) Catecholato Complexes with 4-(2,6-Dimethylphenyliminomethyl)pyridine. Structure, Redox Properties: The Influence of Pyridine Ligand. *J. Organometal. Chem.* **2019**, *897*, 32–41. [[CrossRef](#)]
80. Regan, C.J.; Walton, D.P.; Shafaat, O.S.; Dougherty, D.A. Mechanistic Studies of the Photoinduced Quinone Trimethyl Lock Decaging Process. *J. Am. Chem. Soc.* **2017**, *139*, 4729–4736. [[CrossRef](#)]
81. Berger, S.; Hertl, P.; Rieker, A. Physical and chemical analysis of quinones. In *The Quinonoid Compounds*; Patai, S., Rappoport, Z., Eds.; John Wiley & Sons Ltd.: New York, NY, USA, 1988; pp. 29–78.
82. Amorati, R.; Fumo, M.G.; Menichetti, S.; Munnanini, V.; Pedulli, G.F. Electronic and Hydrogen Bonding Effects on the Chain-Breaking Activity of Sulfur-Containing Phenolic Antioxidants. *J. Org. Chem.* **2006**, *71*, 6325–6332. [[CrossRef](#)]



83. Smolyaninov, I.V.; Poddel'skiy, A.I.; Berberova, N.T.; Cherkasov, V.K.; Abakumov, G.A. Electrochemical transformations of catecholate and *o*-amidophenolate complexes with triphenylantimony(V). *Russ. J. Coord. Chem.* **2010**, *36*, 644–650. [[CrossRef](#)]
84. Smolyaninov, I.V.; Antonova, N.A.; Poddel'skiy, A.I.; Smolyaninova, S.A.; Osipova, V.P.; Berberova, N.T. Radical scavenging activity of sterically hindered catecholate and *o*-amidophenolate complexes of LSb<sup>V</sup>Ph<sub>3</sub> type. *J. Organometal. Chem.* **2011**, *696*, 2611–2620. [[CrossRef](#)]
85. Poddel'skiy, A.I.; Smolyaninov, I.V. 3,6-Di-*tert*-butylcatecholates of triaryl antimony(V): NMR study and redox-transformations. *Russ. J. Gen. Chem.* **2010**, *80*, 538–540. [[CrossRef](#)]
86. Poddel'skiy, A.I.; Ilyakina, E.V.; Smolyaninov, I.V.; Fukin, G.K.; Berberova, N.T.; Cherkasov, V.K.; Abakumov, G.A. Complexes of triphenylantimony(V) catecholates with ammonium salts. Spectroscopic and electrochemical investigations. *Russ. Chem. Bull.* **2014**, *63*, 923–929. [[CrossRef](#)]
87. Poddel'skiy, A.I.; Smolyaninov, I.V.; Kurskii, Yu.A.; Berberova, N.T.; Cherkasov, V.K.; Abakumov, G.A. New dioxygen-inert triphenylantimony(V) catecholate complexes based on *o*-quinones with electron-withdrawing groups. *Russ. Chem. Bull.* **2009**, *58*, 532–537. [[CrossRef](#)]
88. Poddel'skiy, A.I.; Astaf'eva, T.V.; Smolyaninov, I.V.; Arsenyev, M.V.; Fukin, G.K.; Berberova, N.T.; Cherkasov, V.K.; Abakumov, G.A. Triphenylantimony(V) 6-alkoxymethyl-3,5-di-*tert*-butylcatecholates. Structure and redox-properties. *J. Organometal. Chem.* **2018**, *873*, 57–65. [[CrossRef](#)]
89. Poddel'skiy, A.I.; Smolyaninov, I.V.; Fukin, G.K.; Berberova, N.T.; Cherkasov, V.K.; Abakumov, G.A. 3,6-Di-*tert*-butylcatecholates of trialkyl/triarylantimony(V). *J. Organometal. Chem.* **2018**, *867*, 238–245. [[CrossRef](#)]
90. Poddel'skiy, A.I.; Smolyaninov, I.V.; Fukin, G.K.; Berberova, N.T.; Cherkasov, V.K.; Abakumov, G.A. Triarylantimony(V) catecholates—derivatives of 4,5-difluoro-3,6-di-*tert*-butyl-*o*-benzoquinone. *J. Organometal. Chem.* **2016**, *824*, 1–6. [[CrossRef](#)]
91. Poddel'skiy, A.I.; Smolyaninov, I.V.; Berberova, N.T.; Fukin, G.K.; Cherkasov, V.K.; Abakumov, G.A. Triaryl/trialkylantimony(V) catecholates with electron-acceptor groups. *J. Organometal. Chem.* **2015**, *789*, 8–13. [[CrossRef](#)]
92. The Potential Value for 2,6-di-*tert*-butyl-4-methylphenol: 1.48 V vs. Ag/AgCl (GC-electrode, CH<sub>2</sub>Cl<sub>2</sub>). measured in this study.
93. Emsley, J. *The Elements*; Clarendon Press: Oxford, UK, 1991.
94. Easyspin 5.2.25. Available online: <http://www.easyspin.org/> (accessed on 1 July 2019).
95. Perrin, D.D.; Armarego, W.L.F.; Perrin, D.R. *Purification of Laboratory Chemicals*; Pergamon: Oxford, UK, 1980.
96. Bruker; SAINT. *Data Reduction and Correction Program v.8.27B*; Bruker AXS: Madison, WI, USA, 2012.
97. Bruker; SADABS. *Bruker/Siemens Area Detector Absorption Correction Program, v.2014/2*; Bruker AXS: Madison, WI, USA, 2014.
98. Sheldrick, G.M. *SHELXTL. Structure Determination Software Suite, v.6.14*; Bruker AXS: Madison, WI, USA, 2003.

**Sample Availability:** Samples of the compounds are available from the authors.



© 2020 by the authors. Licensee MDPI, Basel, Switzerland. This article is an open access article distributed under the terms and conditions of the Creative Commons Attribution (CC BY) license (<http://creativecommons.org/licenses/by/4.0/>).